

# Enhanced recovery and non-linear dynamics in the wake of a model floating offshore wind turbine submitted to side-to-side and fore-aft motion

Thomas Messmer<sup>1</sup>†, Michael Hölling<sup>1</sup>, and Joachim Peinke<sup>1</sup>

<sup>1</sup>ForWind - Center for Wind Energy Research, University of Oldenburg, Institute of Physics, 26129 Oldenburg, Germany

(Received xx; revised xx; accepted xx)

An experimental study in a wind tunnel is presented to explore the wake of a floating wind turbine subjected to harmonic side-to-side and fore-aft motions under laminar inflow conditions. The wake recovery is analysed as a function of the frequency of motion, measured by the Strouhal number,  $St$ . Our findings indicate that both directions of motion accelerate the transition to the far-wake compared to the fixed turbine. The experimental outcomes confirm the CFD results of Li *et al.* (2022) showing that sideways motions lead to faster wake recovery, especially for  $St \in [0.3, 0.6]$ . Additionally, we find that fore-aft motions also lead to better recovery for  $St \in [0.3, 0.9]$ . Moreover, we see that the recovery is closely linked to non-linear spatio-temporal dynamics. Special non-linear dynamical effects are found in the shear layer region of the wake ( $y \approx R$ ). For both directions of motion and  $St \in [0.25, 0.55]$ , the noisy wake dynamics synchronise to the frequency of the motion. For fore-aft motions and  $St \in [0.55, 0.9]$ , the wake shows more complex quasi-periodic phenomena. In fact, the driven frequency and a self-generated meandering mode emerge and interact non-linearly, as proved by occurring mixing components. Sideways motions result in large spatial structures of meandering. Fore-aft motions induce pulsing of the wake. Both modes are linked to the synchronisation effect. The quasi-periodic phenomena of fore-aft motions are connected to meandering mode. Overall, the spatio-temporal phenomena lead to faster recovery likely due to an increase of momentum transport towards wake centre.

**Key words:** Authors should not enter keywords on the manuscript, as these must be chosen by the author during the online submission process and will then be added during the typesetting process (see <http://journals.cambridge.org/data/relatedlink/jfm-keywords.pdf> for the full list)

## 1. Introduction

The worldwide installed capacity of offshore wind is significantly growing since 2010. Most of the current offshore wind turbines are mounted on fixed structures and are clustered in wind farms installed in water depths lower than 60 meters (Díaz & Soares 2020). For water depth larger than 60 meters, floating wind is the preferred solution (Hannon *et al.* 2019). Compared to a fixed turbine, a floating offshore wind turbine

---

† Email address for correspondence: thomas.messmer@uni-oldenburg.de

(FOWT) is free to move in its 6-degree-of-freedom (DoFs). The action of wind, waves and current is responsible of complex platform motions (Jonkman & Matha 2011). These motions depend among others on platform types, environmental conditions, moorings and water depth (Butterfield *et al.* 2007; Goupee *et al.* 2014). The effect of these motions on the aerodynamic of the rotor and the development of the wake is an active research topic becoming highly relevant for wind farms layout.

Typical distances between offshore turbines within a farm in the main direction of the wind are in the range of  $6D$  to  $12D$  (Hou *et al.* 2019). This implies that downstream turbines operate in the wake of upstream turbines. The wake of an offshore turbine is a high-turbulent and low energy flow region compared to the undisturbed flow. There is thus a lot of interest to understand the evolution of the wake of a wind turbine and especially the features of the far-wake (typically for  $x/D \geq 6$ ). Over the past decades, several numerical studies, theoretical models, field measurements and wind tunnel experiments have been carried out, leading to significant progress in the rich subject of fixed wind turbine wakes (Ainslie 1988; Vermeer *et al.* 2003; Chamorro & Porté-Agel 2009; Porté-Agel *et al.* 2020; Neunaber *et al.* 2020).

(i) *Wake regions of a fixed wind turbine.* As the study of the wake of a FOWT prerequisites a good knowledge of the wake of a fixed turbine, we start a discussion of wake features of a fixed turbine. Recent work by Neunaber *et al.* (2020) depicts in great details the different regions in the wake generated by a wind turbine. The **near-wake** is located in the vicinity of the turbine, characterised by the presence of hub-, root- and tip-vortices (Vermeer *et al.* 2003). These vortices are advected downstream by the mean flow, until instabilities occur, which lead to the destruction of the vortex system. The complex mechanisms that lead to the destruction of the coherent structures are extensively described in (Widnall 1972; Felli *et al.* 2011; Lignarolo *et al.* 2015). Lignarolo *et al.* (2015) confirmed the hypothesis of Medici (2005) regarding the fact that the tip-vortices shield the wake from the outer flow and prevent the exchange of momentum that provides re-energisation to the wake. The process of recovery thus starts when the tip vortices become unstable, which marks the beginning of the **transition region**. At that point, the shear layer which separates the wake to the undisturbed flow grows radially. Momentum is transported from the outer region to the wake and turbulence builds up in the wake. When the shear layers merge at the center, the amount of turbulence in the wake is at its maximum and then gradually decrease as moving downstream (similar to the behaviour of the wake of a fractal grid as shown by Hurst & Vassilicos (2007)). At this specific point, the wind speed along the hub center line begins to recover. This area is the **decay region**. Finally, when turbulence in the wake has reached an homogeneous-isotropic state (Pope 2000), the **far-wake** region kicks-off. The size of each region, the intensity of the recovery and the turbulence of the wake depends greatly on the type of inflow and the operating conditions of the turbine (Wu & Porté-Agel 2012; Iungo *et al.* 2013; Neunaber *et al.* 2017). It is clear that the emergence of the far-wake are directly linked to the phenomena that happened in the regions closer to the rotor, however in the center of the far-wake the detailed features of its turbulence seem to be universal. The breakdown of tip-vortices generate small-scale turbulence that transports momentum from the surroundings to the wake, thus being an important mechanism for the recovery of the wake (Lignarolo *et al.* 2015).

(ii) *Wake meandering of a fixed wind turbine.* An important property of the wake of a wind turbine is its tendency to oscillate mainly side-to-side, so-called wake

meandering (Medici & Alfredsson 2006; Larsen *et al.* 2008; Howard *et al.* 2015). This phenomenon originates from two different causes: on the one hand, the turbulent flow of the atmosphere contains large eddies whose scale is larger than the wake width. These large eddies pass through the rotor and are responsible for the low frequency and large amplitude oscillation of the wake (Larsen *et al.* 2008; Espana *et al.* 2011; Heisel *et al.* 2018). On the other hand, wake instabilities can cause meandering in the far-wake, where the wake tends to oscillate at a frequency,  $f_m$  expressed in terms of Strouhal number,  $St_m = f_m D / U_\infty \in [0.1, 0.5]$ . Observations from various studies, such as Okulov *et al.* (2014); Foti *et al.* (2018); Heisel *et al.* (2018); Gupta & Wan (2019), have revealed a broad peak in the spectra at  $f_m$ , which indicates that wake oscillations differ from classical vortex shedding, which typically exhibits a sharp peak at the shedding frequency. After Gupta & Wan (2019) wake meandering occurs in the far-wake due to the “amplification of upstream disturbances by shear flow instabilities”. Perturbations around the natural frequency of wake meandering,  $f_m$  can cause an early onset of meandering (Mao & Sørensen 2018; Gupta & Wan 2019).

(iii) *Wake of a floating wind turbine.* The latest topic of floating wind turbines raises fundamental questions about the impact of movements on the development of the wake. Another aspect not further discuss here is the impact on rotor aerodynamic. Firstly, the motions of a floating turbine are responsible for unsteady aerodynamic phenomena. Unsteadinesses are observed for high frequency of motions, characterised by the dimensionless Strouhal number,  $St = f_p D / U_\infty$  (where  $f_p$  is the frequency of motion,  $D$  is the rotor diameter, and  $U_\infty$  is the inflow speed), typically for  $St > 0.5$  (Sebastian & Lackner 2013; Farrugia *et al.* 2014; Sant *et al.* 2015; Bayati *et al.* 2017a; Fontanella *et al.* 2021). Secondly, rotor motions impact wake dynamics, which was shown through various wind tunnel studies with model turbines and porous disks (Rockel *et al.* 2014, 2017; Bayati *et al.* 2017b; Fu *et al.* 2019; Schliffke *et al.* 2020; Kopperstad *et al.* 2020; Fontanella *et al.* 2022; Meng *et al.* 2022; Belvasi *et al.* 2022). Bayati *et al.* (2017b) discussed the relevance of the so-called “wake reduced velocity”, which is equivalent to a Strouhal number, for the characterisation of unsteady aerodynamic conditions. Fu *et al.* (2019) measured with PIV the wake of a pitching and rolling model turbine with rather high amplitudes (up to  $20^\circ$ ) an low frequencies ( $St < 0.03$ ). They observed a stronger recovery for the floating turbine and enhanced Turbulent Kinetic Energy (TKE), which was also observed by Rockel *et al.* (2017). A more systematic study was carried out by Schliffke *et al.* (2020) in which they measured at 4.6D downstream the wake of a surging porous disc with  $St \in [0, 0.24]$  under realistic turbulent conditions. No impact of motions on the recovery of the wake was measured, however a signature of the motions in the spectra of the wake was observed for all frequencies. Kopperstad *et al.* (2020) investigated in a wind tunnel and with CFD the wake of a spar and barge floating turbine. They showed that in a laminar wind, the wake of a floating turbine recovers faster compared to a fixed machine, for which the recovery depends on the wave excitation. Numerical simulations using free-wake vortex code and CFD were carried out to study the different wake regions of a floating turbine (Farrugia *et al.* 2016; Lee & Lee 2019; Chen *et al.* 2022; Kleine *et al.* 2022; Chen *et al.* 2022; Li *et al.* 2022; Ramos-García *et al.* 2022). Farrugia *et al.* (2016) outlined the possibility for surge motion “to induce the onset of complex interactions between adjacent tip vortices”. These instabilities induced by surge motion on the complex helical vortex system could explain the faster recovery of the wake of a surging turbine for a range of  $St \in [0.4, 1.7]$ , studied by Ramos-García *et al.* (2022). Based on stability theory of vortices, Kleine *et al.* (2022) showed that the motion of a floating turbine “excites vortex instabilities modes”,

which were predicted by Farrugia *et al.* (2016). They demonstrated that motions with a frequency of 0.5 and 1.5 the rotor 1P frequency induce the strongest disturbances. Chen *et al.* (2022) carried out CFD simulations of the wake of a surging turbine with amplitude  $A_p \in [0.03D, 0.1D]$ ,  $St \in [0.41, 1.64]$ . They showed the positive impact of motions on the recovery of the wake of a surging turbine, where up to 10 % more recovery compared to the fixed turbine was found. Last but not least, Li *et al.* (2022) used CFD to study the onset of wake meandering arising from the sideways motion of a floating turbine. They demonstrated that sway motions for  $St \in [0.2, 0.6]$  helps the wake to recover up to 20 % more compared to fixed case. They showed that side-to-side turbine motions lead to large wake meandering, even with small amplitude of motions ( $A_p/D \approx 0.01$ ). This important result is particularly pronounced for low turbulent conditions ( $TI < 4\%$ ).

The above mentioned discussion shows that the current understanding of the wake of floating wind turbines is based on many specific investigations. In Pimenta *et al.* (2021) we reported on p.4-5 on wind tunnel experiments that we conducted in 2021 on cases similar to Li *et al.* (2022). In this paper, we extended our experiments to side-to-side and fore-aft harmonic motions to obtain a more global understanding of the wake development for different types of movements of a FOWT. A special focus is given to the influence of the frequency of movements. In order to examine solely the impact of the motion on the wake and to exclude any impact of inflow turbulence, the turbine was operated in laminar wind. In this work, we addressed the following questions:

- (i) Which non-dimensional numbers and principle directions of motion drive the wake dynamics of a floating wind turbine?
- (ii) How do side-to-side and fore-and-aft movements affect the development of the far wake of a floating turbine? Is there a range of motion frequencies that allows the wake of a moving turbine to recover faster? What are the underlying mechanisms?

The §2 details the experimental set-up, the cases investigated and the methodology for the analysis. The §3 presents the averaged results, i.e the profiles of wake deficit and turbulence intensity. Here we show the dependency to the DoF on the wake. We describe the effects of side-to-side motions with  $St \in [0, 0.58]$  and fore-aft motions with  $St \in [0, 0.97]$  on the wake recovery. The §4 examines the dynamics of the wake and discusses the results in terms of non-linear dynamics.

## 2. Experiments

### 2.1. Set-up

The experimental set-up used to perform the investigations is shown in figure 1. The experiments were done in the  $3 \times 3 \text{ m}^2 \times 30 \text{ m}$  test section of the large wind tunnel of the University of Oldenburg (Kröger *et al.* 2018). The set-up consists of the Model Wind Turbine Oldenburg 0.6 (MoWiTO 0.6) with a diameter of  $\sim 0.6 \text{ m}$  mounted on a motorised platform.

A 6-DoF motorised platform was designed specifically for the MoWiTO 0.6 in order to investigate the aerodynamic of FOWTs (Messmer *et al.* 2022). With this system, the model turbine can be moved following pre-defined motion signals in the 6 degree-of-freedom, namely the three translations: surge, sway and heave and the three rotations: roll, pitch and yaw. The model turbine was equipped with a strain gage to measure the thrust,  $T$ , of the ensemble {tower + rotor}. For any case investigated: power produced,

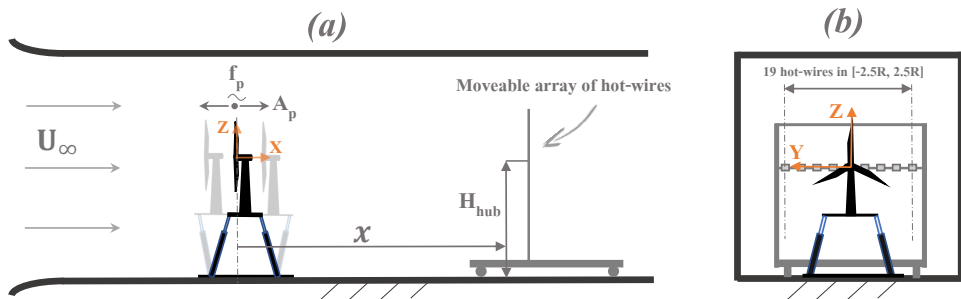


FIGURE 1. Scheme of the experimental set-up, the MoWiTO 0.6 mounted on a 6-DoF platform installed in the wind tunnel (a) side view and (b) front view. *not to scale*

rotational speed and thrust of the turbine was recorded. The movements of the platform were recorded to verify the adequacy of the motions. The wind speed,  $U$ , in the wake of the model turbine was measured with an array of 19 1-dimensional hot-wires of  $\sim 1\text{mm}$  length, resolving turbulent scale of this size.

The probes were operated with multichannel 54N80-CTA (Constant Temperature Anemometer) modules from *Dantec Dynamics*. Data were acquired with a sampling rate of 6 kHz, gathering  $\sim 10^6$  points for each measurement. The time of measurements,  $T_{meas}$  was sufficient to reach statistical convergence of any post-processed data shown and discussed in this paper. The hot-wire probes were calibrated twice daily and temperature, humidity and air pressure were recorded throughout the day to track any drift effects, which came out to be negligible. The inflow wind speed was measured with a Prandtl-tube about two meters in front of the model turbine.

The array was mounted on a moving motorised cart which allowed to measure the wind speed, at the downstream position,  $x$ , from 6D to 10D (cf figure 1 (a)). We selected this range of distances based on the typical layout of a wind farm as mentioned in §1. The hot-wires were placed on a horizontal line at hub-height (around 1 meter above floor level) and span lateral positions,  $y$  from  $-2.5R$  to  $2.5R$  ( $R = D/2$ ) with respect to the hub centre (cf figure 1 (b)).

## 2.2. Model Wind Turbine Oldenburg 0.6

The MoWiTO 0.6 used for the experiments has a rotor diameter,  $D$  of 0.58 m. The turbine is developed at the University of Oldenburg (Schottler *et al.* 2016; Jüchter *et al.* 2022). The properties of the turbine are depicted in appendix A in table 2. The model turbine was used for several measurement campaigns with a focus on wake flow, further details of the experimental procedure and wake measurements can be found in Hulsman *et al.* (2020); Neunaber *et al.* (2020, 2022).

The turbine used for the measurements was characterised by power and thrust coefficients ( $C_P$ ,  $C_T$ ) vs Tip Speed Ratio ( $TSR$ ). Figure 2 (a) displays  $C_p$  vs.  $TSR$  and figure 2 (b)  $C_T$  vs.  $TSR$  for  $U_\infty = 3, 5$  m/s resulting in a rotor-based Reynolds number,  $Re$  from  $1.4 \times 10^5$  to  $2.3 \times 10^5$ . The power coefficient is  $Re$  dependent. For  $TSR \approx 6$ ,  $C_p$  increases from 0.2 at low  $Re$  to 0.30 at the highest  $Re$ . This is consistent with the features of the low- $Re$  airfoil used, SD7003, which performs better at high  $Re$  (Selig 1995). The thrust coefficient is around 0.8 for  $TSR \approx 6$ . The thrust coefficient account for rotor and tower aerodynamic loads. In a previous study by Neunaber *et al.* (2020), the load on the

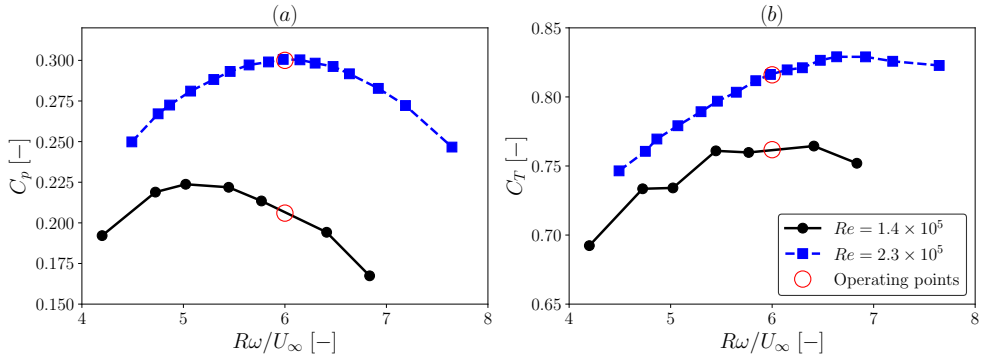


FIGURE 2.  $C_P$  (a) and  $C_T$  (b) versus tip speed ratio of the MoWiTO 0.6 for two rotor-based Reynolds number (for  $U_\infty = 3, 5$  m/s) at fixed blade pitch angle

Thrust coef.	Power coef.	Tip Speed Ratio	Reduced amplitude	Strouhal number	Reynolds number
$C_T$	$C_P$	$TSR$	$A^*$	$St$	$Re$
$\frac{T}{1/2\rho\pi R^2 U_\infty^2}$	$\frac{P}{1/2\rho\pi R^2 U_\infty^3}$	$\frac{R\omega}{U_\infty}$	$\frac{A_p}{D}$	$\frac{f_p D}{U_\infty}$	$\frac{\rho U_\infty D}{\eta}$

TABLE 1. Dimensionless parameters that drive the wake of a FOWT

tower and nacelle of the MoWiTO 0.6 was measured without the blades. The authors assessed this value to be 17 % of the total thrust coefficient. The operating points of the wake experiments are marked by red circles in figure 2. All measurements were carried out at  $TSR \approx 6$  for which  $C_T \approx 0.76$  at 3 m/s and  $C_T \approx 0.81$  at 5 m/s.

### 2.3. Non-dimensional parameters that drive the wake behaviour

As for our desired experiment investigations many quantities are involved, we briefly discuss the selection of necessary parameters for a complete characterisation. Therefore we use the basis of the  $\pi$ -theorem. For a given DoF, the system investigated involves a total of nine independent parameters, namely platform motion frequency and amplitude, inflow wind speed, rotor diameter, air viscosity, air density, turbine thrust and power and rotational speed. These are noted:  $f_p, A_p, U_\infty, D, \mu, \rho, T, P, \omega$ . The  $\pi$ -Theorem suggests that, a problem characterised by  $m$  dimensional variables can always be reduced to a set of  $m-n$  dimensionless parameters ( $\pi$ -groups), with  $n$  the fundamental units of measure (dimensions) as depicted by Buckingham (1914). Therefore this problem with nine variables and three dimensions can be reduced to six dimensionless parameters. These are all defined in table 1, namely the thrust coefficient,  $C_T$ , power coefficient,  $C_P$ , tip speed ratio,  $TSR$ , reduced amplitude,  $A^*$ , Strouhal number,  $St$ , and Reynolds number,  $Re$ . Thus in a laminar flow, the properties of the wake of a FOWT,  $wake_{FOWT}$ , are determined by these six dimensionless numbers:  $wake_{FOWT} = f(C_T, C_P, TSR, A^*, St, Re)$ .

The dependency to  $C_T$  of wake recovery and expansion of a wind turbine was characterised extensively (Porté-Agel *et al.* 2020). The tip speed ratio also plays an important role on the development of the wake of a FOWT (Farrugia *et al.* 2016). Both the amplitude and frequency of motions can impact the wake of a moving turbine, as demonstrated by Chen *et al.* (2022); Li *et al.* (2022); Ramos-García *et al.* (2022). As

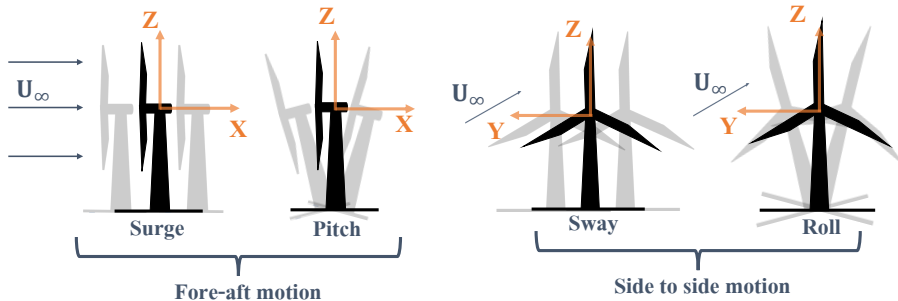


FIGURE 3. Fore-aft (surge and pitch) and side-to-side motions (sway and roll) of a FOWT

already mentioned above, motion frequency has a greater influence on wake dynamics, even at low amplitudes ( $A_p \sim 0.01D$ ). Based on these works and the set of parameters, we concluded that it is worth to focus on the impact of different  $St$  at constant amplitude of motions.

#### 2.4. Cases investigated

Floating wind turbines operate in the atmospheric boundary layer, which exhibits various turbulent conditions, typically  $TI \in [2, 15]$  (Jacobsen & Godvik 2021; Angelou *et al.* 2023). The complex conditions (6-DoF motions and turbulent conditions) of a floating wind turbine were idealised for the experiments. We considered laminar wind with a low background turbulent intensity of  $\sim 0.3\%$ , and imposed 1-DoF harmonic motions. Our study focused on investigating the four following DoFs: surge, sway, roll, and pitch for a specific range of  $St$ . Figure 3 illustrates the four DoFs, with fore-aft and side-to-side motions. We examined these DoFs independently, without combining them. We imposed for a given DoF the following motion signal,  $\xi$ , on the platform:  $\xi(t) = A_p \sin(2\pi f_p t)$ . Here,  $A_p$  denotes the amplitude of motion (in meters or degrees), and  $f_p$  represents the frequency of motion (in Hz).

In order to investigate a relevant range of  $St$ , we looked at the typical movements of a FOWT, which we briefly present below. The motions of a floating wind turbine are greatly influenced by the type of foundation used (TLP, semi-submersible and spar). Three distinct ranges of frequencies are usually observed in the motion spectra of a floating turbine:

(i) *Wave frequency*: a floating platform is subject to ocean waves which cause motions at frequencies around 0.1 Hz (wave period around 10 s). Although the wave-induced motions are rather low in amplitude ( $A^* \sim 0.01$ ), they are high in frequency. For a 10 MW turbine at rated wind speed, typically  $St \sim 1.5$  (Messmer *et al.* 2022).

(ii) *Rotational natural frequency*: when a floating turbine is displaced from its equilibrium position (due to a gust or a series of waves), it goes back to equilibrium as a damped harmonic oscillator at a frequency that depends on the degree of freedom. For a spar or a semi-submersible, the pitch and roll natural frequencies are typically around 0.035 Hz (Robertson *et al.* 2014). For a 10 MW turbine at rated wind speed, such motions give  $St \sim 0.5$  and  $A^*$  up to  $\sim 0.04$ .

(iii) *Translation natural frequency*: similar to rotational degrees of freedom, a floating turbine experiences translation motions at natural frequencies. These can be large in amplitude ( $A^*$  up to  $\sim 0.1$ ) but at low frequency ( $f_p \sim 0.01$  Hz). Typical Strouhal number is  $St \sim 0.1$  (Leimeister *et al.* 2018).

This discussion demonstrates that floating turbines cover range of Strouhal numbers,  $St \in [0, 1.5]$ . While high-frequency movements are relatively low in amplitudes ( $A^* \sim 0.01$ ), oscillations at lower frequencies can reach amplitudes up to 10% of the rotor diameter. To test a wide range of  $St$ , we conducted experiments at frequencies ranging from 0.3 to 5 Hz with a constant amplitude of motion around  $0.01D$ . We considered two inflow wind speeds: 3 and 5 m/s and set the rotational speed of the turbine using a torque controller to maintain a  $TSR$  of approximately 6.0 for all cases. We covered  $St \in [0, 0.97]$ . Table 3 in Appendix A provides details on all the cases investigated.

To quantify the differences between the cases, we took as reference the fixed case ( $St = 0$ ). To make this study of our different cases comparable, it is important to note that the mean power and thrust of the moving turbine were the same as those of the fixed turbine. If this would not have been the case, comparing the wake flows between cases would be less meaningful, as there would be differences in mean operating conditions.

It was also confirmed by examining the wake deficit in the near-wake, which was the same for any case with the same Reynolds number,  $\langle C_T \rangle$ ,  $\langle C_P \rangle$ , and  $\langle TSR \rangle$ . With this we concluded that the induction factor of the turbine was the same, which was also observed by Fontanella *et al.* (2022). In particular for the fore-aft motion, such a result is not obvious as motions cause temporal variations in turbine power and thrust. We found that they do not affect the mean turbine output values, at least for such low amplitudes. However, the impact of the motions is directly related to their effects on the dynamics of the wake (added turbulence and non-linearities).

### 2.5. Post-processing of measured data

In order to quantify the different wake measurements, we analysed the time series of local wind velocity by one- and two-dimensional statistics and by their instantaneous flow fields, defined hereafter. The measured time series are given in the form of  $U(x, y, z = z_{hub}, t)$  with  $x \in [6D, 8D, 10D]$ ,  $y \in [-2.5R, 2.5R]$  and  $t \in [0, T_{meas} \approx 180$  s].  $\langle \cdot \rangle$  denotes a temporal average for  $t \in [0, T_{meas}]$ .

**Normalised wind speed deficit (wake deficit)** is quantified by  $\Delta U(x, y)/U_\infty = (U_\infty - \langle U(x, y, t) \rangle)/U_\infty$ . In the paper, we show profiles of wind deficit, the closer the deficit to zero the more the wake has recovered.

**Wind recovery ( $\sim$  rotor normalised averaged wind speed)** is defined as  $\tilde{U}/U_\infty$ , where  $\tilde{U}(x) = \int_{y_0-R}^{y_0+R} \langle U(x, y, t) \rangle dy$ . With  $y_0$  the estimated center of the wake. This quantity gives an order of magnitude of the amount of wind speed that has recovered at a specific downstream position around the rotor area, similar quantity were calculated by Chen *et al.* (2022); Li *et al.* (2022). In this paper, we also refer to  $\tilde{U}/U_\infty$  as the recovery.

**Turbulence intensity** is given by  $TI(x, y) = \sigma(U(x, y, t))/\langle U(x, y, t) \rangle$

**Power spectra**,  $\Phi_x(x, y)$ , is the power spectral density of the wind speed fluctuations,  $u(x, y, t) = U(x, y, t) - \langle U(x, y, t) \rangle$  computed with an algorithm that uses Welch's method.



**Instantaneous wind field** is based on  $U(x, y, z = z_{hub}, t)$  to visualise the instantaneous wake at hub height for a specific case and downstream position. A low-pass filter with a cut-off frequency of 10 Hz was applied to remove small-scale fluctuations from the signals for each  $y$  value within the range of  $[-2.5R, 2.5R]$ . The signals were then resampled at a frequency of 500 Hz and plotted on a colormap (see §4).

**Cross-correlation between  $U(x, y = -1/2R, t)$  and  $U(x, y = 1/2R, t)$**  is given by  $(U_{-1/2R} \star U_{1/2R})(\tau) = \langle U(y = -1/2R, t)U(y = 1/2R, t + \tau) \rangle / \sigma_{-1/2R}\sigma_{1/2R}$

### 3. Results of average values

The scheme after which we present our results is briefly explained next. We considered four DoFs, for which wake measurements are compared. The analysis of the wakes are done for the three downstream positions ( $x \in \llbracket 6D, 8D, 10D \rrbracket$ ). The downstream dependency of the cross stream-wise profiles of wake velocity deficit and turbulence intensity is shown. Finally the recoveries of the wakes are analysed with respect to the  $St$ .

We begin this section by presenting, in §§3.1, the similarity between degrees of freedom that led us to reduce the analysis to two generic DoFs namely sway and surge. Then, the dependency of the wake recovery on the  $St$  is shown in §§3.2 for sway. Finally, we present corresponding results for surge motions in §§3.3.

#### 3.1. Equivalence between different degrees of freedom

In a previous study from Bayati *et al.* (2017a), the authors simplified the modelling of the aerodynamics of a FOWT by linearising rotational motions into translation. We checked whether this simplification is also applicable to sway/roll motions or respectively to surge/pitch motions.

To address this issue, we measured the wake of the floating turbine with small ( $A_p = 0.5^\circ$ ) and large ( $A_p = 5^\circ$ ) amplitudes of platform roll around the zero value. Additionally, we performed tests with the turbine swaying at an equivalent amplitude. We carried out the same tests with pitch and surge DoFs (with no tilt angle). The results of side-to-side motions (sway and roll) are presented in figure 4, while the fore-aft motions are shown in figure 5. The wind speed deficit and turbulence intensity profiles are plotted for 6D, 8D, and 10D in figures (a-c) and (d-e), respectively.

For the sway and roll cases, figure 4 demonstrates that the match of  $\Delta U/U_\infty$  and  $TI$  is nearly perfect both low amplitudes ( $A^* = 0.007$ ) and high amplitudes ( $A^* = 0.065$ ). This suggests that the Bayati approximation can be applied also for the wake for these types of motions.

Figure 5 demonstrates that for low-amplitude cases ( $A^* = 0.007$ ), the wind speed deficit and turbulence intensity profiles of the wake are very similar for pitch and surge. However, for larger amplitudes ( $A^* = 0.065$ ), discrepancies arise. The wake of a surging turbine at low frequency ( $St < 0.1$ ) has little impact on the wake, even at high amplitude (see figure 5, the blue curves marked with triangles follow closely the fixed case marked by black line with dots). This is consistent with the results of Meng *et al.* (2022). In contrast, the equivalent case with pitch motion (see the blue curve with squares) clearly deviates from the fixed case. After Rockel *et al.* (2017); Fu *et al.* (2019), the deviations observed are due to vertical wake movements induced by the rotor tilting. The wake of a pitching turbine is similar to that of a surging turbine only for low amplitudes ( $A_p < 2^\circ$ ) as seen in figure 5 by the results marked with the red diamond and star symbols.

Our findings allowed us to simplify the study by focusing only on sway for side-to-side

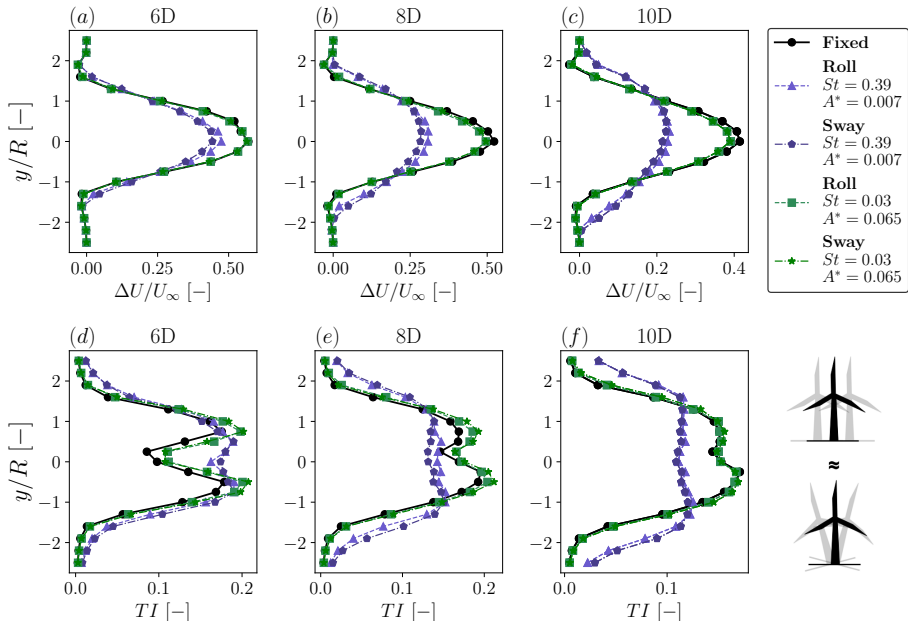


FIGURE 4. Wake deficit (a-c) and TI profiles (d-f) at 6D, 8D and 10D for fixed case and two roll and sway cases with same  $St$  and same  $A^*$ ,  $Re = 2.3 \times 10^5$ . Tests A.1-5 in table 3

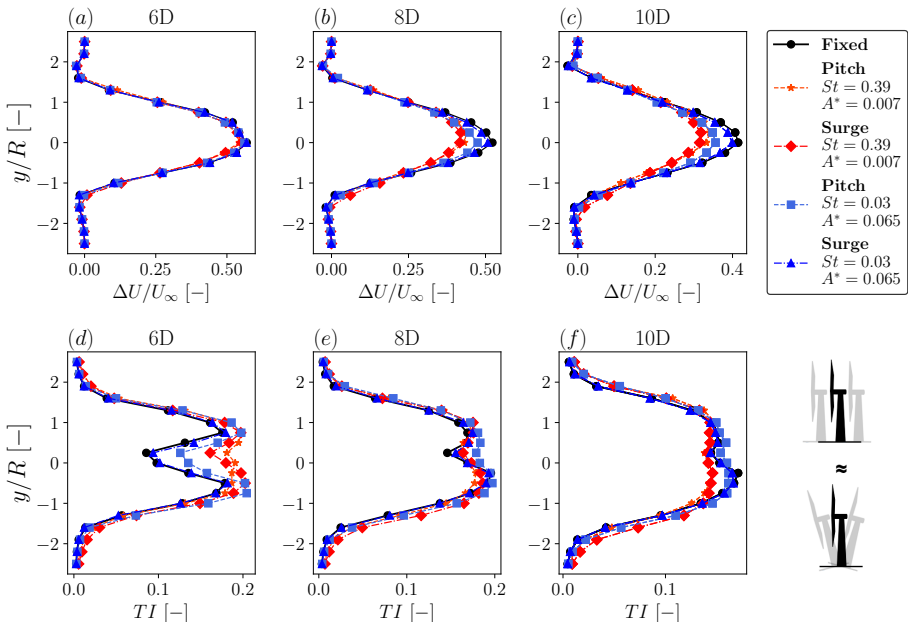


FIGURE 5. Wake deficit (a-c) and TI profiles (d-f) at 6D, 8D and 10D for fixed case and two pitch and surge cases with same  $St$  and same  $A^*$ ,  $Re = 2.3 \times 10^5$ . Tests B.1-5 in table 3

motions and surge for fore-aft motions. We can extend the conclusions of these DoFs to pitch and roll motions, as long as the equivalent amplitude is below a certain value, which we estimate to be around  $2^\circ$ , i.e.  $A^* \approx 0.025$ .

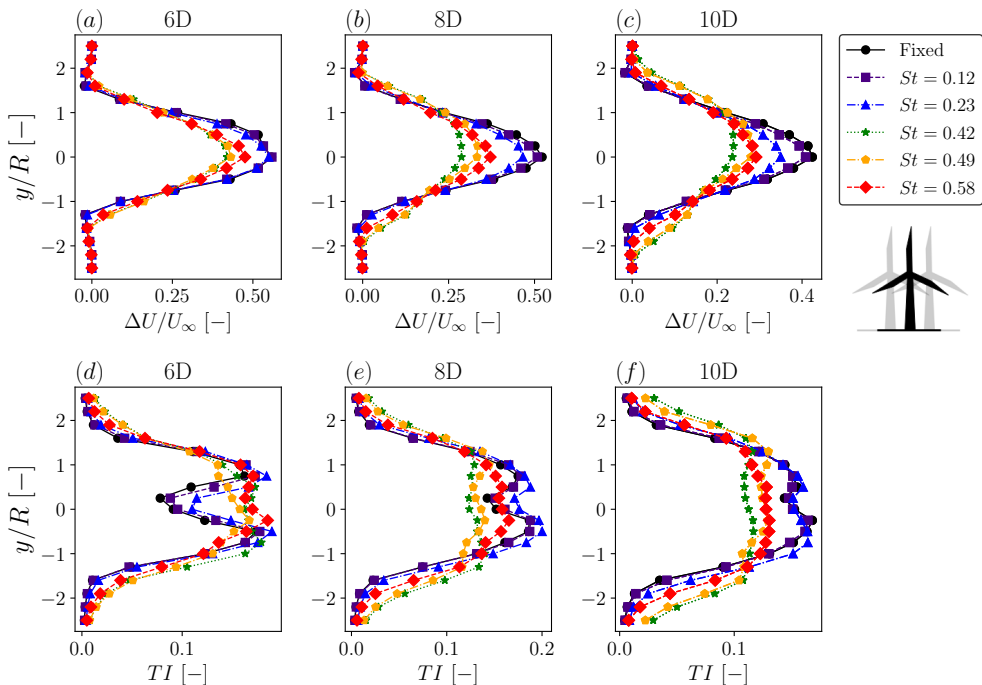


FIGURE 6. Wake deficit (a-c) and  $TI$  profiles (d-f) at 6D, 8D and 10D for fixed case and five sway cases with varying  $St$  and constant  $A^* = 0.007$ ,  $Re = 2.3 \times 10^5$ . Tests C.1-2 in table 3

### 3.2. Sway motion

From the results presented in §§3.1 (figure 4) we already see that the wake is strongly influenced by the  $St$  (frequency of the motion). We observe that a higher frequency leads to a better wake recovery. To investigate the  $St$  dependency, we measured the wake for different platform motion frequencies at constant amplitude ( $A^* = 0.007$  and  $St \in [0.12, 0.58]$ ) similar to the CFD simulations done by Li *et al.* (2022).

Figure 6 shows the wake deficit and turbulence intensity ( $TI$ ) profiles at 6D, 8D, and 10D for the fixed case and five sway cases. Most interestingly, we find that for  $St = 0.42$  the wake has the lowest deficit (figure 6 (b,c) green stars). Similar results are observed for the profiles of  $TI$ , see figure 6 (e,f). Another interesting effect of wakes, discussed for instance by Porté-Agel *et al.* (2020), is the merging of the shear layers characterised by the vanishing of the two peaks in the profile of  $TI$ . In figure 6 (d-f), it can be seen that the merging occurs for fixed and  $St < 0.25$  between 8D and 10D. In contrast, the merging is found already around 6D for higher  $St$ .

To quantify the impact of motion frequency on the wind speed recovery, we computed  $\bar{U}(x)/U_\infty$ , as explained in §§2.5. Figure 7 shows our results together with the CFD simulations of Li *et al.* (2022). Although the two dataset are obtained for quite different  $Re$ , they match very well. We found that for each downstream position, the amount of wind recovered gradually increases up to a maximum for  $St \approx 0.4$ , after which it decreases. Sway movements of the turbine positively impact the recovery in the range of  $St \in [0.3, 0.6]$ , but the impact is less important outside of this range and approaches that of fixed case as  $St \searrow 0$ . Comparing the results between  $St = 0$  (fixed) and  $St \approx 0.4$  (optimum) we found differences up to 25 % in the recovery, this means that a wind turbine downstream could produced in this case ( $St \approx 0.4$ ) significantly more power.

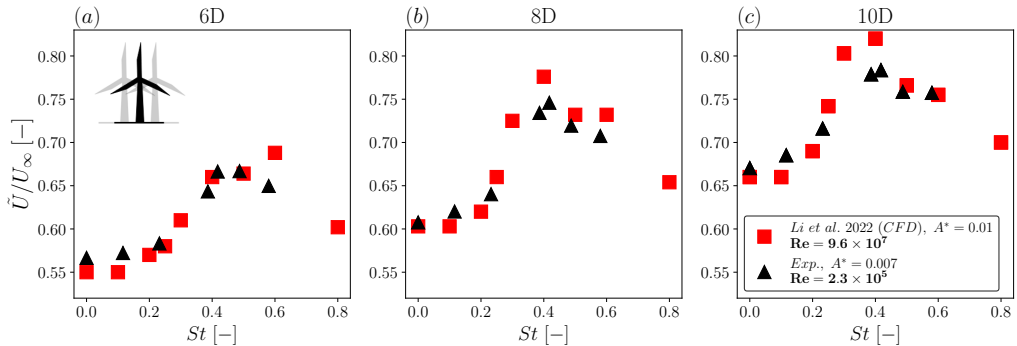


FIGURE 7. Wake recovery expressed by the normalised average wind speed in the rotor area,  $\tilde{U}/U_\infty$ , defined in §§2.5 at 6D (a), 8D (b) and 10D (c) for fixed case and seven **sway** cases with varying  $St$  and constant  $A^* = 0.007$ ,  $Re = 2.3 \times 10^5$ . Tests C.1-2 in table 3. Also plotted with red squares: equivalent data from CFD simulations by Li *et al.* (2022), for which  $A^* = 0.01$ ,  $Re = 9.6 \times 10^7$  and  $C_T$  unknown

### 3.3. Surge motion

We then present the results of the surge motions in a manner comparable to that of the sway. Based on a first experiment, we concluded about the necessity to investigate higher values of  $St$  than for sway. In fact, we observed a plateau in the recovery for  $St > 0.5$ , which differs to the behaviour with sway motion (figure 7). Thus we carried out experiments with  $St \in [0, 0.97]$ . To achieve this range of  $St$ , we used an inflow wind speed,  $U_\infty$ , of 3 m/s, see table 3 (tests D.1-2).

The wake deficit and  $TI$  profiles are shown in figure 8. Notably, the wake for  $St = 0.81$  has the lowest deficit, see profiles marked by yellow pentagons in figure 8 (b,c). Likewise, the profile of  $TI$  is the lowest at 10D for  $St = 0.81$  (figure 8 (f)). The merging of the shear layers occur at around 6D for  $St \in [0.5, 0.8]$  (figure 8 (d)) and between 8D and 10D for other cases.

We also did the same experiments with  $U_\infty = 5$  m/s, with which we could investigate  $St$  up to 0.58 (D.3-4 in table 3). We thus have results for two  $Re$ , respectively  $Re = 1.4 \times 10^5$  and  $Re = 2.3 \times 10^5$ . We calculated  $\tilde{U}(x)/U_\infty$  (cf §§2.5), to quantify the recovery with respect to  $St$  as shown in figure 9. For each position, the recovery increases for  $St \in [0, 0.6]$ , stays almost constant for  $St \in [0.6, 0.8]$  and then decreases. Both  $Re$  show comparable results.

### 3.4. Discussion

The results show that, for both surge and sway motions,  $St$  has a significant impact on wake recovery. Sway provides the highest wake recovery in the range of  $St$  in  $[0.3, 0.6]$  (figure 7). For surge case, the high recovery range extends to higher  $St$  values, namely in  $[0.3, 0.9]$ . Sway shows an optimal recovery well centred at  $St^{opt} \approx 0.4$ , whereas for surge the optimum is spread over a range of  $St^{opt} \in [0.5, 0.8]$ . Therefore, we conclude that the dynamical behaviour of the wake is likely to differ depending on the degree of freedom (DoF).

Concerning the  $TI$ , the merging of the shear layers is an important property of the wake, which provides information about the wake development. We found that both types of motion cause an early merging (around 6D) compared to fixed case (between 8D and 10D), see  $TI$  profiles in figures 6 (d) and 8 (d). Additionally, the maximum value of  $TI$  is higher for the motion cases (up to 20 % more than the fixed case). This indicates that movements generate extra turbulence in the form of small-scale turbulence as well as

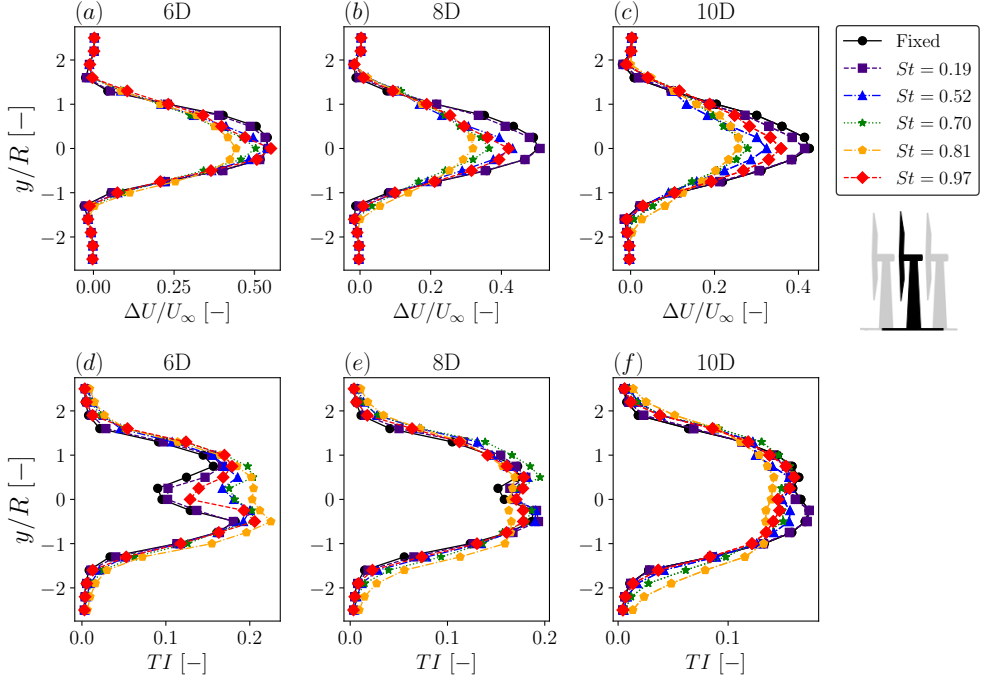


FIGURE 8. Wake deficit (a-c) and  $TI$  profiles (d-f) at 6D, 8D and 10D for fixed case and five surge cases with varying  $St$  and constant  $A^* = 0.007$ ,  $Re = 1.4 \times 10^5$ . Tests D.1-2 in table 3

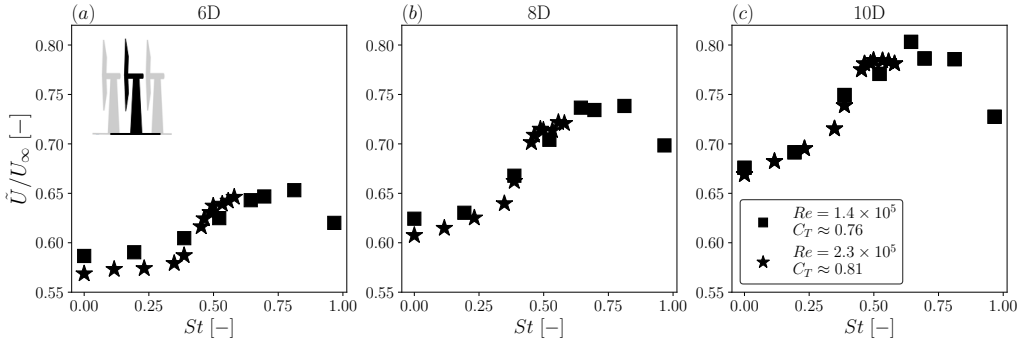


FIGURE 9. Wake recovery expressed by the normalised average wind speed in the rotor area,  $\tilde{U}/U_\infty$ , defined in §§2.5 at 6D (a), 8D (b) and 10D (c) for fixed case and various surge cases with varying  $St$ , constant  $A^* = 0.007$  and two  $Re$ :  $1.4 \times 10^5$ ,  $2.3 \times 10^5$ . Tests D.1-4 in table 3

coherent structures, which accelerate the transition from near- to far-wake (as detailed later in the paper).

Figure 7 shows the recovery for two  $Re$  ( $Re \sim 10^8$  from CFD and  $Re \sim 2 \times 10^5$  in the experiments). Despite great differences in  $Re$ , the results match very well. For surge, we found that the recovery is similar for  $Re = 1.4 \times 10^5$  and  $Re = 2.3 \times 10^5$  (see figure 9). So we conclude that the wake of a floating turbine do not depend sensitively on  $Re$ , at least for  $Re > 10^5$ .

The results of §3 motivated us for further investigations on the time resolved structures of the wakes, presented next in §4.

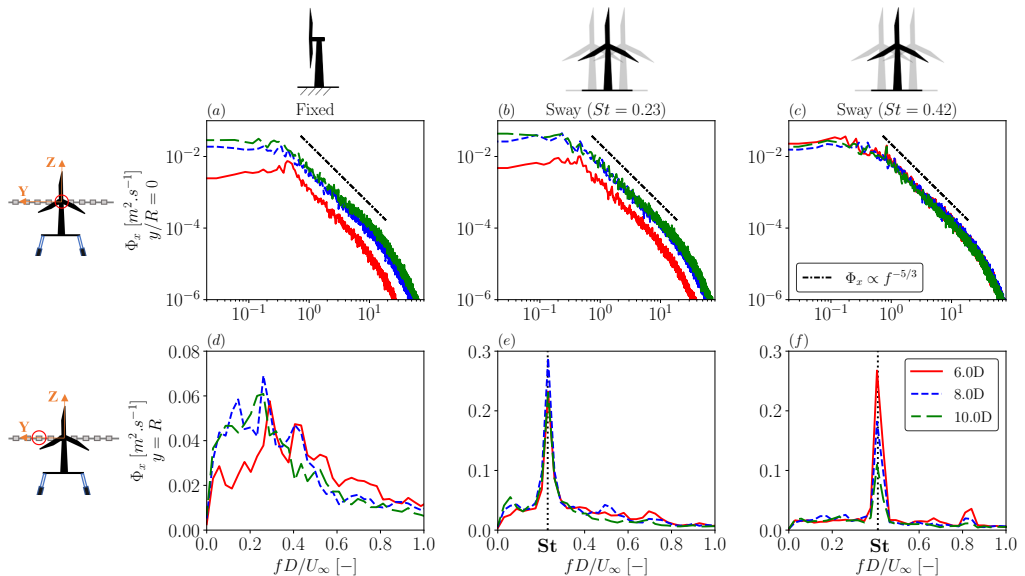


FIGURE 10. Power spectra of the wind speed fluctuations in the wake at 6-10D for fixed case (a, d) and two **sway** cases ( $St = 0.23$  (b, e) and  $St = 0.42$  (c, f)) at two locations ( $y/R = 0$  on top) and ( $y = R$  on bottom).  $A^* = 0.007$ ,  $Re = 2.3 \times 10^5$ . Tests C.1-2 in table 3

## 4. Wake dynamics

In the following §§4.1 and §§4.2, we present the impact of the movements on the dynamics of the wake flow for sway and surge motions respectively. We then discuss these results in terms of non-linear dynamics in §§4.3.

### 4.1. Wake dynamics under sway motion

During a sway motion cycle, wakes are generated at various horizontal positions spanning  $y \in [-A_p, +A_p]$ . The mixing and interactions of these “multiple” wakes affect the mean wake. For low frequencies, the wakes emitted at different horizontal positions superpose linearly (as shown in figure 17 in appendix A and Meng *et al.* (2022)). As in our case, we are interested in small amplitudes ( $A^* \sim 0.01$ ) we assume that this linear superposition holds true if the profiles of  $\Delta U/U_\infty$  and  $TI$  coincide the fixed case. Clear deviations are interpreted as a non linear response. As seen in figure 6, for  $St = 0.12$ , the profiles match well the fixed case, but is not the case for higher  $St$ .

To further investigate the wake generated by the swaying turbine, we computed the power spectra,  $\Phi_x$  (see §§2.5 for details) from the hot-wire measurements of the local velocity time series. Figure 10 displays  $\Phi_x$  computed at  $y = 0$  (a-c) and  $y = R$  (d-f) for the following cases: fixed (a,d),  $St = 0.23$  (b,e),  $St = 0.42$  (c,f) for  $x \in [6D, 8D, 10D]$ . For  $St = 0.42$ , the spectra along the centreline all collapse for  $fD/U_\infty > 1$ , see figure 10 (c). In the inertia sub-range ( $fD/U_\infty \in [1, \sim 20]$ ),  $\Phi_x \propto f^{-5/3}$ , which shows that turbulence in the wake center is fully developed (Pope 2000; Neunaber *et al.* 2020). Thus, the far-wake is reached at  $x \leq 6D$  for  $St = 0.42$ , which is in line with the merging of the shear layers seen in figure 6 (d).

For  $St = 0.23$ , the spectra at  $x = 8D$  and  $x = 10D$  merged, indicating that the far-wake region is reached between 6D and 8D. For the fixed case, all three spectra are unequal, showing that the far-wake first appears at  $x > 8D$ .

At  $y = R$ , the spectra of the fixed turbine display a region of high turbulent energy

for  $fD/U_\infty \in [0.1, 0.5]$ , showing the presence of flow structures with characteristic frequencies in this range (figure 10 (d)). At  $x = 6D$ , the highest energy is contained in  $f_m D/U_\infty \approx 0.35$ . According to Foti *et al.* (2018), the far-wake of a wind turbine experiences meandering at a natural frequency, typically in the range of  $f_m \in [0.1, 0.5]U_\infty/D$ . Gupta & Wan (2019) further explains that the inherently erratic wake tends to amplify small perturbations, resulting in wake meandering far downstream. The broad peak at  $f_m D/U_\infty$  is consistent with this explanation, suggesting that such meanderings result from shear flow instabilities. These instabilities span a range of frequencies and do not show a clear peak, as would be typical for vortex shedding.

The spectra of moving cases show a distinct peak at the frequency of movements for all downstream positions, see figure 10 (e,f). This peak is a signature of the motions within the wake, indicating that the far-wake contains coherent structures at the frequency of the motion. This was also observed by Fu *et al.* (2019) and Li *et al.* (2022). This pseudo lock-in phenomenon, as described in Gupta & Wan (2019), occurs when the wake flow synchronises with the forcing frequency imposed by the periodic upstream perturbation (in our case the movements of the platform). Pseudo lock-in is observed when the platform's motion frequency,  $f_p$ , is around  $f_m$ , and seems to be the strongest when  $f_p$  is closest to  $f_m$ . The intensity of the lock-in is highest at  $x = 6D$  for  $St = 0.42$ . For other cases, the highest lock-in occurs at  $x = 8D$ , indicating a spatial dependency. From the spectra analysis, we can conclude that the wake dynamics are closely following the motions frequency.

The array of hot-wires, with 19 probes aligned horizontally, enables visualisation of the instantaneous wake flow of the turbine (see §§2.5 for details). Figure 11 shows the time evolution of  $U(x, y, t)$  for the fixed case (a,d,g),  $St = 0.23$  (b,e,h), and  $St = 0.42$  (c,f,i) at the three downstream positions. For the fixed case, time (x-axis) is multiplied by  $f_m \approx 0.35U_\infty/D$ . In the case of the moving turbine, time is multiplied by the frequency of motion of the platform.

For the above mentioned case of the highest lock-in response ( $St = 0.42$  at  $x = 6D$ ) we see correspondingly a clear meandering pattern at the imposed frequency,  $f_p$  (figure 11 (c)). As we move downstream, the amplitude of meandering increase and the structures become more fuzziier.

For lower  $St$  of 0.23, we see how the structures seem to be a combination of the flows of the fixed case and  $St = 0.42$ . For fixed and  $St = 0.23$ , the meandering structures become more prominent for larger distances.

Overall, the clearest meandering structures are obtained for  $St = 0.42$  quite close to the rotor ( $x = 6D$ ). Whereas the other cases have a tendency to build up less clear meandering structures only further downstream.

Coming back to the profiles of wake deficit, we found that the wake expansion is the largest for  $St = 0.42$  (figure 6 (b, c)), which coincides with the biggest meandering amplitudes of the wake field (figure 11 (c,f,i)). In figure 7, we define the wake recovery over a range of  $y \in \sim [-R, R]$ , which corresponds to the energy available for a virtual turbine operating in this wake. If a larger range is considered, the recovery is less significant but still higher. From our time-resolved measurements, we find that, compared to the fixed case, the swaying motions of the platform enhance the sideways motion of the wake, which distributes the momentum more evenly within  $y \in [-2.5R, 2.5R]$ . The larger surface area of the wake as well its dynamics enable more transport of momentum to the center of the wake.

The spectra in figure 10 is not a complete characterisation of a meandering wake. However, the instantaneous wake flow fields in figure 11 clearly indicate meandering. To

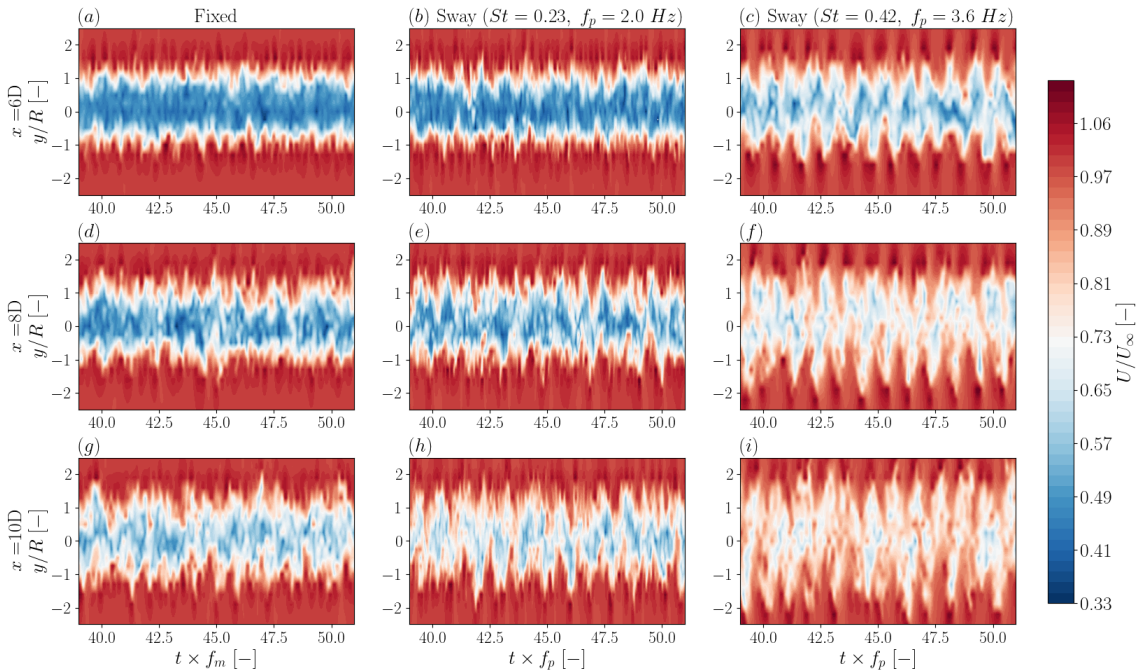


FIGURE 11. Instantaneous wind field in the wake at 6-10D for fixed case (a,d,g) and two **sway** cases ( $St = 0.23$  (b,e,h) and  $St = 0.42$  (c,f,i)).  $A^* = 0.007$ ,  $Re = 2.3 \times 10^5$ . Tests C.1-2 in table 3. For fixed case, time is multiplied by  $f_m = 0.35 \times U_\infty/D$ . For moving cases, time is multiplied by  $f_p$ .

further quantify the meandering at a given frequency, we calculated the cross-correlation function (depicted in §2.5) between  $U(x, -1/2R, t)$  and  $U(x, 1/2R, t + \tau)$  for  $\tau$  varying from 0 to  $3/f_p$ . Figure 12 shows this quantity computed at 6D (a), 8D (b), and 10D (c) for both fixed and a few swaying cases. We plot  $(U_{-1/2R} \star U_{1/2R})(\tau)$  versus  $\tau \times f_p$ , except for the fixed case where we set  $\tau \times f_p = \tau$ . In figure 12 (a), it can be seen that for  $St \in [0.2, 0.5]$ ,  $(U_{-1/2R} \star U_{1/2R})(\tau)$  is a harmonic function with a period equal to the platform's oscillation period,  $1/f_p$ , consistent with the pseudo lock-in phenomenon. The function attains its minimum value (negative value) at  $\tau \approx 0$ . For  $x = 6D$  and  $St = 0.42$ , the minimum value of  $(U_{-1/2R} \star U_{1/2R})(\tau \approx 0)$  is approximately  $-0.3$ , which indicates that the signals  $U(-1/2R, t)$  and  $U(1/2R, t)$  are anti-correlated. This anti-correlation quantifies the side-to-side motion of the wake at a specific frequency. When the wake meanders to the left,  $U(1/2R, t)$  decreases and  $U(-1/2R, t)$  increases and vice versa (for illustration see figure 12 (g)). Consistently, the correlation is maximal at  $\tau \approx 1/2f_p$ .

In figure 12 (d-f),  $(U_{-1/2R} \star U_{1/2R})(\tau \approx 0)$  is plotted vs.  $St$  for the three downstream positions. In figure 12 (d), the anti-correlation is significant in the range of  $St \in [0.2, 0.5]$  and close to zero for other values, confirming the range of motion frequencies that initiate large wake meandering.

#### 4.2. Wake dynamics under surge motion

Surge motions, unlike sway motions, induce variations of  $C_T$  that affect the dynamics of the overall wake.  $C_T$  oscillates at  $f_p$  and is out of phase of around  $\pi/2$  with the signal of motions as shown by Fontanella *et al.* (2021). So  $C_T(t) = \langle C_T \rangle + \Delta C_T \sin(2\pi f_p t + \phi)$ , with  $\Delta C_T$  the amplitude of thrust oscillation and  $\phi$  the phase shift with the signal of



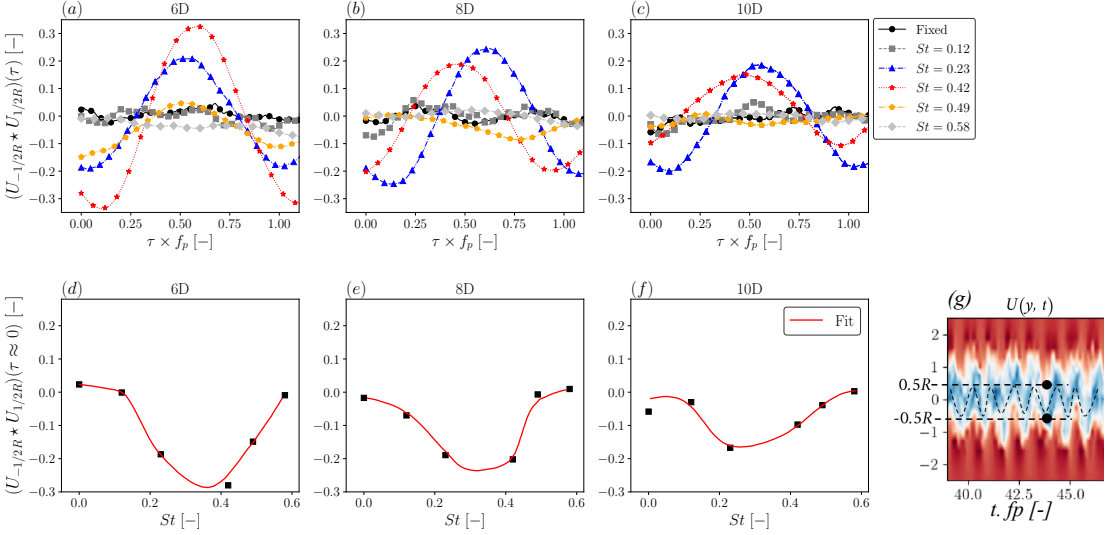


FIGURE 12. Cross-correlation between  $U(x, -1/2R, t)$  and  $U(x, 1/2R, t + \tau)$ , noted  $(U_{-1/2R} \star U_{1/2R})(\tau)$ , for fixed case and **sway** cases with varying  $St$  at 6-10D (a,b,c). Plot of  $(U_{-1/2R} \star U_{1/2R})(\tau \approx 0)$  vs.  $St$  (d-f).  $A^* = 0.007$ ,  $Re = 2.3 \times 10^5$ . Tests C.1-2 in table 3. (g) is an illustration of the cross-correlation for  $\tau = 0$ .

motion. In our case, the highest value of thrust coefficient variation is:  $\Delta C_T^{max} \approx 0.07$  for  $f_p = 5$  Hz,  $A_p = 0.004$  m,  $U_\infty = 3$  m/s. Besides the  $C_T$  variations, the wake is generated behind the turbine at various  $x$  locations spanning  $[-A_p, +A_p]$  during one cycle of motion.

As for sway, when  $St < 0.1$ , the wake of the surging turbine is similar to that of the fixed turbine, even at high amplitude (see figure 5 (c)), which is consistent with Schliffke *et al.* (2020); Meng *et al.* (2022); Belvasi *et al.* (2022). When the frequency is higher,  $St > 0.2$ , the interactions of the wakes emitted at different  $x$  positions and with different  $C_T$  become more complex.

To understand the impact of surge movements on the dynamics of the wake we carried out a similar analysis to that made for sway (§§4.1). Figure 13 shows the power spectra of fixed (a,d), surge with  $St = 0.38$  (b,e) and surge with  $St = 0.81$  (c,f) for the three downstream positions at  $y = 0$  (a-c) and  $y = R$  (d-f).

The spectra of  $St = 0.81$  at  $y = 0$  all collapsed to one spectra for  $fD/U_\infty > 1.0$ , and  $\Phi_x \propto f^{-5/3}$  (for  $fD/U_\infty \in [1, \sim 20]$ ) which confirms that the far-wake is reached even for  $x \leq 6D$ . Whereas for the lowest  $St$  and the fixed case, the the far-wake is developed for larger distances,  $x > 6D$ . This behaviour is very similar to that observed for the swaying turbine.

$\Phi_x$  at  $y = R$  exhibit a pronounced peak at the motion frequency ( $St$ ) for both surge cases, in line with results from Schliffke *et al.* (2020); Belvasi *et al.* (2022). As for sway, this indicates that the wake of the surging turbine contains coherent flow structures with a characteristic frequency of  $f_p$ . The peak is for both  $St$  maximum at  $x = 6D$  and then decreases.

When looking at the spectra of the fixed turbine at  $y = R$ , the frequency range with the largest amount of energy is similar ( $0.1 < fD/U_\infty < 0.5$ ) to that of the other fixed case in figure 10 (d). The maximum energy is located at  $f_m \approx 0.3U_\infty/D$ , which is close to than in figure 10 (d). These two cases have a  $Re$  from  $2.3 \times 10^5$  in figure 10 to  $1.4 \times 10^5$

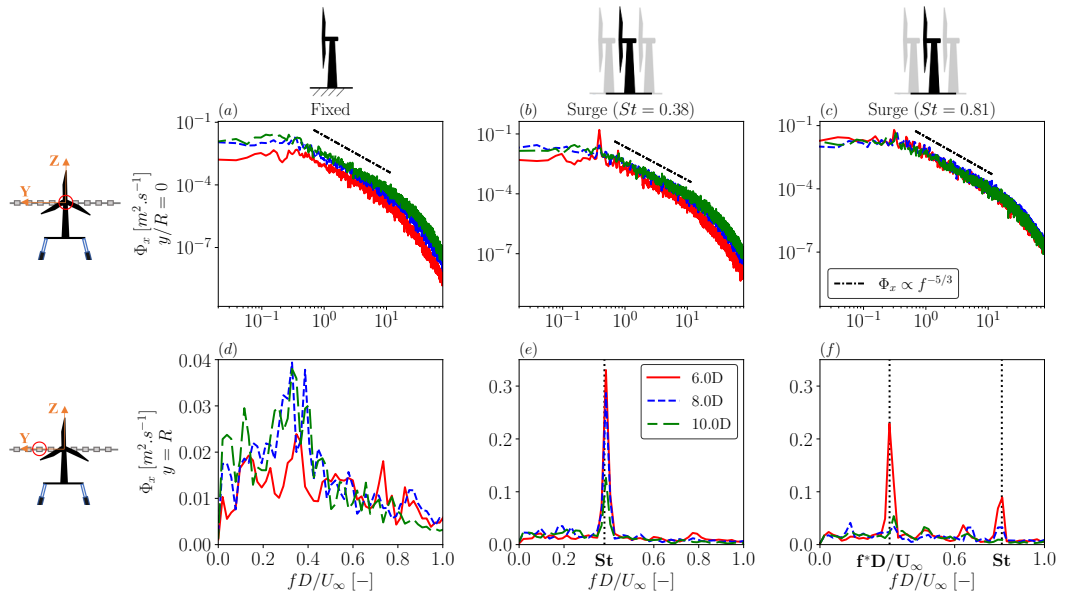


FIGURE 13. Power spectra of the wind speed fluctuations in the wake at 6-10D for fixed case (a, d) and two **surge** cases ( $St = 0.38$  (b, e) and  $St = 0.81$  (c, f)) at two locations ( $y/R = 0$  on top) and ( $y = R$  on bottom).  $A^* = 0.007$ ,  $Re = 1.4 \times 10^5$ . Tests D.1-2 in table 3

in figure 13.

Looking at the case of  $St = 0.38$ , we see interestingly that all frequency components of the fixed case merge to one narrow peak corresponding to the excitation frequency with  $St = 0.38$ . This is somehow similar to the sway cases (see figure 10 (e,f)). For  $St = 0.81$ , compared to the sway case, a new dynamical behaviour is observed, namely we find two frequencies in the spectra with apparent mixing components. One peak is at the excitation frequency, i.e.  $St = 0.81$ . The other peak at  $0.31U_\infty/D$  seems to be due to a self generated mode,  $f^*$  of the wake (around  $f_m$ , the meandering frequency of the fixed turbine). Most interestingly, the further smaller peaks are related to linear combinations of the two frequencies, i.e. with  $a(f^*D/U_\infty) + bSt$ . One small peak is around (a,b) = (1,-1/2) and another one at (a,b) = (1,-1). This proves non-linear mode coupling, which is discussed later in §§4.3. For other values of  $St \in [0.6, 0.9]$ , we also observe a second large peak at a frequency,  $f^*$  in  $[0.15, 0.35]U_\infty/D$  like the one at  $0.31U_\infty/D$  for  $St = 0.81$ . It is important to note that the value of  $f^*$  changes with the exciting frequency,  $St$ .

As for sway, we are interested in the spatio-temporal structure of these oscillating modes. We show in figure 14 the instantaneous wake flows field for the three cases: fixed case (a,d,g),  $St = 0.38$  (b,e,h), and  $St = 0.81$  (c,f,i).

The most striking flow pattern is seen at  $x = 6D$  for  $St = 0.38$  (figure 14 (b)). The wake is pulsating at the frequency of the motions. In the wake of the two further downstream positions (figure 14 (e, h)), the pulsing is gradually reduced.

The flow dynamics at  $St = 0.81$  are quite different, the wake at  $6D$  (figure 14 (c)) is clearly meandering with a frequency of  $f^* \approx 0.31U_\infty/D$ , in consistency with the spectra of this case (figure 13 (f)). Further downstream, the periodic structures become more irregular, which is also seen in the reduced peaks in the spectra at  $x = 8D$  and  $x = 10D$ .

To investigate the pulsing and meandering modes of the wake in more details, we computed the cross-correlation between the wind speed signals  $U(x, -1/2R, t)$  and

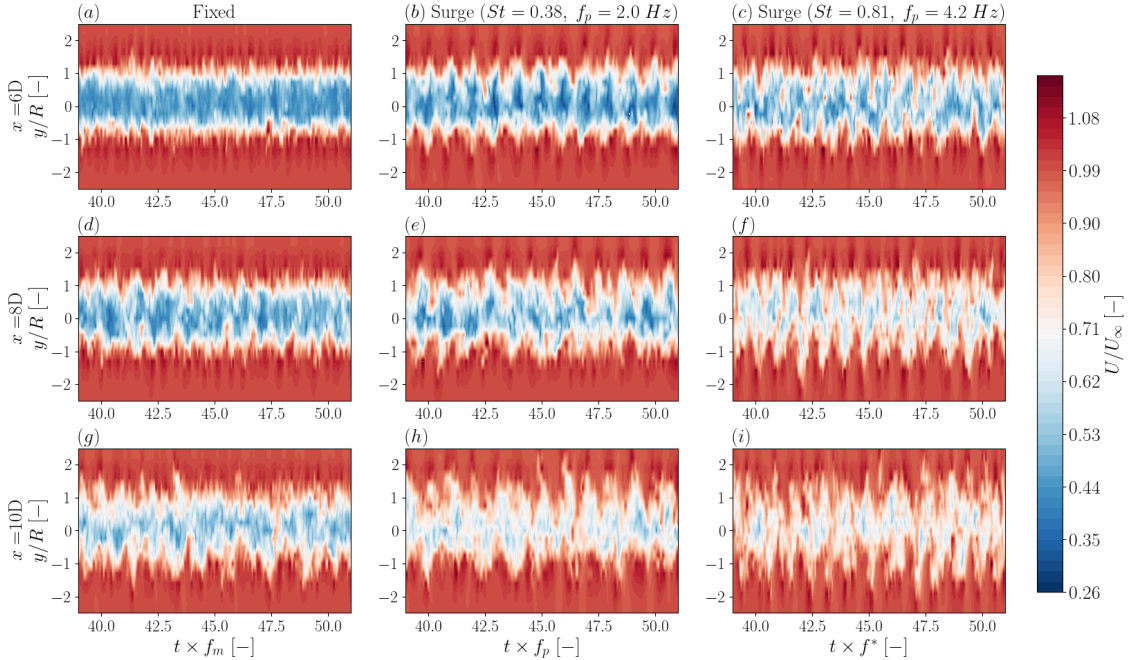


FIGURE 14. Instantaneous wind field in the wake at 6-10D for fixed case (a,d,g) and two surge cases ( $St = 0.38$  (b,e,h) and  $St = 0.81$  (c,f,i)).  $A^* = 0.007$ ,  $Re = 1.4 \times 10^5$ . Tests D.1-2 in table 3. For fixed case, time is multiplied by  $f_m \approx 0.30U_\infty/D$ . For  $St = 0.38$ , time is multiplied by  $f_p$  and for  $St = 0.81$  is multiplied by  $f^* \approx 0.31U_\infty/D$ .

$U(x, 1/2R, t + \tau)$  (cf §2.5). We calculated  $(U_{-1/2R} \star U_{1/2R})(\tau)$  for surge cases E.1-4 (see table 3). Figure 15 shows  $(U_{-1/2R} \star U_{1/2R})(\tau)$  as a function of  $\tau \times f_p$ . In figure 15 (a), we observe that the cross-correlation is almost zero everywhere for  $St < 0.25$  and  $St \approx 1.0$ , indicating that the wake does not oscillate at a clear frequency.

For  $0.25 < St < 0.55$ ,  $(U_{-1/2R} \star U_{1/2R})(\tau)$  is a harmonic function with a period of  $1/f_p$ , and the cross-correlation is maximal (positive) at  $\tau \approx 0$ . The velocity fluctuations between  $y = -1/2R$  and  $y = 1/2R$  are in phase, which implies that the wake undergoes pulsating movements and not meandering.

On the other hand, for  $St = 0.81$ ,  $(U_{-1/2R} \star U_{1/2R})(\tau)$  is a harmonic function with a period of  $\sim D/(0.31U_\infty)$ , and the cross-correlation is minimum (negative) at  $\tau \approx 0$ . This behaviour is associated with meandering movements of the wake at a given frequency, as discussed for sway in §4.1 and is consistent with the instantaneous flow fields shown in figure 14 (c, f, i).

Next we show that the analysis of the cross-correlation functions allows to distinguish the different ranges of  $St$  for which the wake's dynamic behaviour changes. In figure 15 (d-f) the  $St$  dependency of the cross-correlation at  $\tau \approx 0$  is shown. The fit of this cross-correlation allows to identify three distinct regions, highlighted in figure 12 (d) and schematically visualised in figure 12 (g-i). For  $St < 0.25$  and  $St \approx 1.0$  (zone (g)), the motions do not significantly impact the wake's dynamic, which is similar to that of the fixed turbine (as illustrated in figure 15 (g)). For  $St \in [0.25, 0.55]$  (zone (h)), the positive correlation values indicate that the wake undergoes pulsating movements (maximum correlation at  $St \approx 0.4$ ). Picture (h) shows typical pulsating pattern in the wake. For  $St > 0.55$ ,  $(U_{-1/2R} \star U_{1/2R})(\tau \approx 0)$  decreases and becomes negative, indicating that the wake meanders, as shown in picture (i).

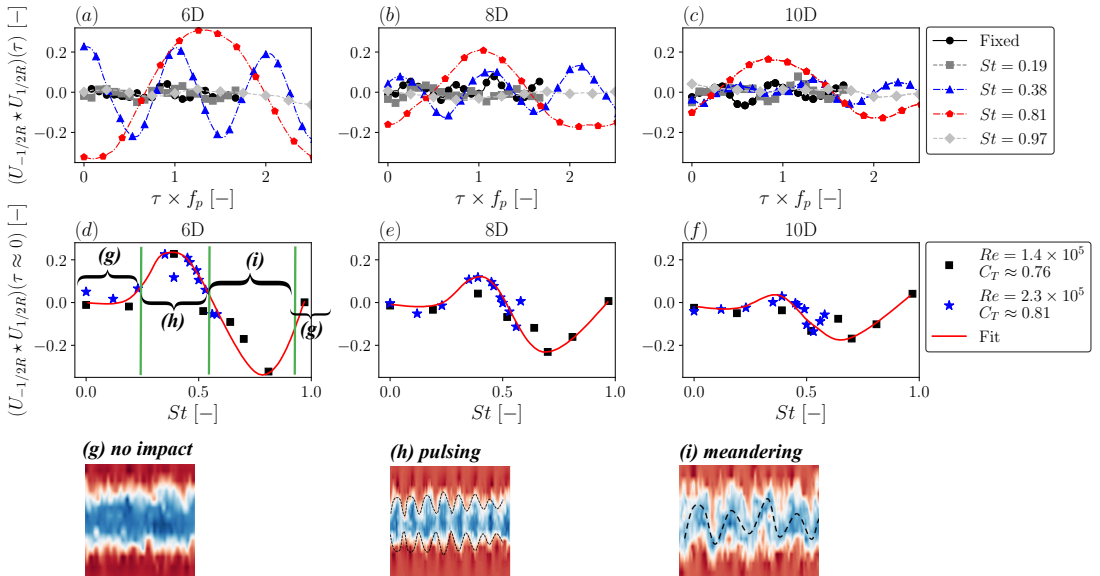


FIGURE 15. Cross-correlation between  $U(x, -1/2R, t)$  and  $U(x, 1/2R, t + \tau)$ , noted  $(U_{-1/2R} \star U_{1/2R})(\tau)$ , for fixed case and **surge** cases with varying  $St$  at 6-10D (a,b,c). Plot of  $(U_{-1/2R} \star U_{1/2R})(\tau \approx 0)$  vs.  $St$  (d-f).  $A^* = 0.007$ ,  $Re = 1.4 \times 10^5$  and  $Re = 2.3 \times 10^5$ . Tests D.1-4 in table 3. *Picture (g) depicts the wake of the fixed turbine, picture (h) shows a typical pulsating motion of the wake and picture (i) displays a typical meandering pattern*

Further downstream, our analysis indicates that pulsating motions as well as the meandering motions gradually vanish. In figure 15 (e,f), the cross-correlation values are overall reduced.

### 4.3. Discussion in terms of non-linear dynamical system

The following discussion concentrates on the boundary region of the wake which is dominated by shear ( $y \approx R$ ). First, we summarise the observations made for the wake of the fixed turbine. For this case, we found a kind of broadband coloured noise in the range of  $fD/U_\infty \in [0.1, 0.5]$  (see figure 10 (d) and figure 13 (d)) with a maximum at about 0.35 which we denoted as meandering frequency,  $f_m$ . As mentioned in the introduction, this broadband noise is consistent with Okulov *et al.* (2014); Foti *et al.* (2018); Heisel *et al.* (2018); Gupta & Wan (2019). These dynamics are most likely the result of the development of shear layer instabilities.

Clear differences in wake dynamics are seen between sway and surge motions. Whereas under sway movements, one clear wake meandering mode is found, we observe two modes for surge, namely a pulsing (for  $St \in [0.25, 0.55]$ ) and a meandering mode (for  $St \in [0.55, 0.9]$ ) as seen in figure 15 (d). The pulsing mode vanishes, or gets damped out, for larger distances ( $x > 8D$ ) as well as for higher  $St$  numbers ( $St > 0.6$ ). Adjacent to this pulsing mode region of low distances and low  $St$ , a smeared-out (turbulent) meandering mode is observed (see figure 14 (b) for clear pulsing, (h) for smeared out pulsing, (c) for clear meandering mode and (i) for more “turbulent” meandering).

These modes can be interpreted in terms of general characteristics of non-linear dynamics (Peinke *et al.* 2012; Argyris *et al.* 2015). The first remarkable feature is the

synchronisation of the wake dynamic to the forcing frequency of the platform motion (see figure 10 (f) for sway and figure 13 (e) for surge). Compared to the spectra of the fixed case, we clearly see how the broad band frequency gets slaved to a narrow band peak (Haken 2012). Such a synchronisation effect, or pseudo lock-in, is a prominent feature of non-linear dynamics discussed in various contexts. It is well known that many coupled pendulums with different frequencies have the tendency to synchronise to one common frequency (Acebrón *et al.* 2005). If so, this suggests that the synchronisation effect is caused by the driving surge or sway motion, which has a similar effect to that of the coupling of the pendulums in the case mentioned above. Another explanation may be given by the so-called stochastic resonance, which describes how a noisy system gets into resonance with a small exciting periodic perturbation (Benzi *et al.* 1981). This is consistent with our observations that the amplitude of the meandering and pulsing due to platform movements ( $\sim 0.01D$ ) is about one to two orders of magnitude larger ( $\sim D$ ) than the platform amplitude, indicating a significant amplification of the small disturbances that grow downstream. Another characteristic of synchronisation is that it is robust to changes in the driving frequency within a finite range. At the end of such a synchronisation range, other non-linear effects emerge. The tracking to the driving frequency is clearly seen for our experiments (see figure 16 (c-f)). In summary, we observe a synchronisation of the dynamics of the boundary region of the wake to the platform motion together with a high amplification of the amplitude. A strong reduction of the broad band structure of the initial frequency (wake of the fixed turbine) and a locking to the exciting frequency is clearly observed for  $St \in [0.25, 0.55]$  for both sway and surge. This effect corresponds to a significant reduction in the wake dynamical degrees of freedom, in the sense that the non-linear dynamic oscillation has a low dimension, with only two degrees of freedom.

In contrast to sway, the surge motion shows further phenomena of non-linear dynamics. In fact, two spatio-temporal wake patterns are observed, namely the pulsing and the meandering mode (figure 15 (h, i)). As discussed above, for surge with  $St > 0.55$ , two frequencies with mixing components are seen in the spectra (figure 13 (f)). This indicates that the wake synchronises to two frequencies, namely the exciting frequency,  $f_p$  and a self-generated narrow band mode,  $f^*$ . A coupling of these frequencies is a clear sign of non-linear dynamics. In figure 16, we show the psd at  $y = R$  and  $x = 6D$  and  $x = 8D$  for a few surge cases with  $St \in [0, 0.97]$ . Very interesting are the spectra of  $St = 0.7$  (g) and  $St = 0.81$  (h). We see a peak at  $St$  and at  $f^*$  (the self-generated mode) as well as mixing components in the form of  $a(f^*D/U_\infty) + bSt$ . For  $St = 0.70$ , for instance, we identify two further peaks with (a,b) = (1,-1) and (a,b) = (1,-2). Such a dynamic is part of the class of quasi-periodic systems, described with the generic model of circle map, which characterises the quite complex and fast changing dynamical behaviour under such non-linearities (Argyris *et al.* 2015). We observe that one time the amplitude of the driving frequency is larger and the other time the amplitude of the self-generated mode is greater (see figure 16 (g)  $x = 6D$  and  $x = 8D$ ). Mixing components occur more or less pronounced, which is similar to previous observations of non-linearities with semi-conductors as shown in figure 3.56 in Peinke *et al.* (2012).

## 5. Summary and conclusion

In this study, we investigated the impact of side-to-side and fore-aft harmonic motions on the wake of a model floating wind turbine in laminar wind. Our research focused on the impact of motion frequency on the wake, with a constant amplitude of movements of

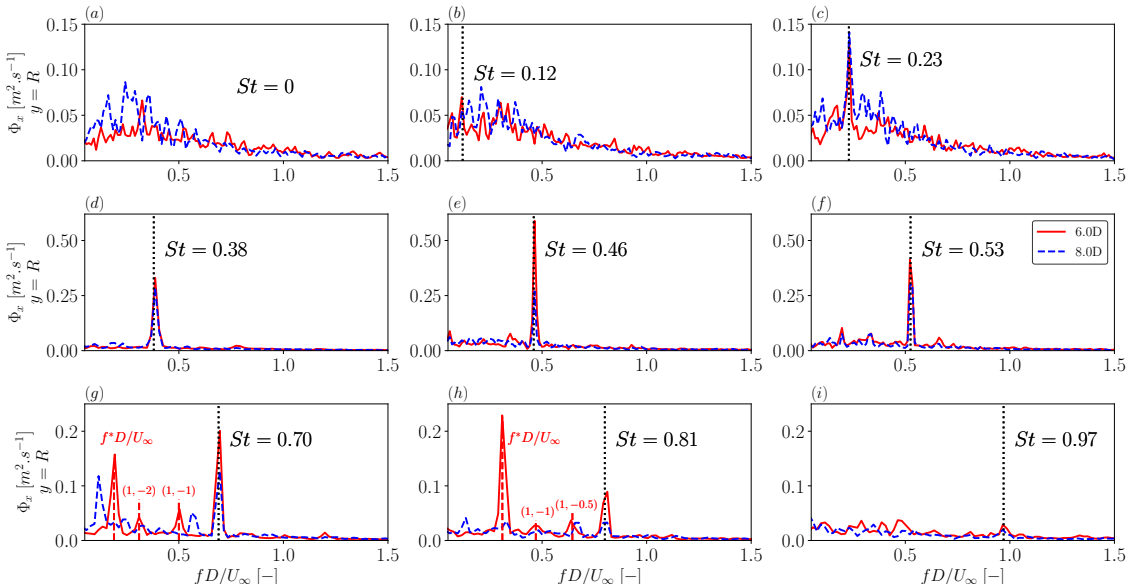


FIGURE 16. Power spectra of the wind speed fluctuations in the wake at  $x = 6D$  and  $x = 8D$  for fixed case (a) and 8 surge cases (b-i) at the location  $y = R$ .  $A^* = 0.007$ ,  $Re = 1.4$  to  $2.3 \times 10^5$ . Tests E.1-4 in table 3

$\sim 0.01D$ . This paper presents a number of new findings. First, our results demonstrate the equivalence between surge and pitch, as well as, between sway and roll (see figures 4 and 5 in §§3.1). Therefore, we focused our research on sway DoF for side-to-side motions and surge DoF for fore-aft. Second, the experimental results are in excellent agreement with the CFD simulations from Li *et al.* (2022) about the wake of a swaying turbine in laminar wind (figure 7). This implies that the wake of the floating turbine does not depend on the Reynolds number, at least for  $Re > 10^5$ . Third, our findings indicate that both types of movement significantly enhance wake recovery, especially for  $St \in [0.3, 0.6]$  with sway (figure 7) and  $St \in [0.3, 0.9]$  for surge (figure 9). Fourth, we worked out different wake modes depending on the direction of motions and  $St$ . For low  $St$  and surge DoF we found a new mode, namely a pulsing mode of the wake. For the same DoF and higher  $St$ , a self generated meandering mode is observed. These are all non-linear dynamical effects.

At such low inflow turbulence, the perturbations induced by the movements of the floating wind turbine are responsible of different dynamics of the wake, which are particularly visible in the shear region of the wake ( $y \approx R$ ). On the one hand, sway motions are inducing large sideways wake meandering, especially for  $St \in [0.2, 0.5]$ . The wake synchronises (pseudo lock-in) to the frequency of movements as seen in the spectrum of the wind fluctuations, which shows a clear and narrow peak at  $f_p$  (see figure 10 (e, f)). The small perturbations induced by the movements are largely amplified and results into clear meandering at  $f_p$  (see figure 11 (c,f)). This dynamical response is a typical non-linear behaviour. Similarly, for  $St \in [0.25, 0.55]$ , the wake of the surging turbine shows pulsating movements at the excitation frequency (see figure 14 (b)). For both DoFs, the broadband frequency range of the wake of the fixed turbine (figures 10 (d) and 13 (d)) is slaved to a single frequency, driven by the motions. This monochromatic response is in some ways much easier to describe than the more complex broadband spectra of the fixed turbine which contains a wide range of flow structures.

On the other hand, for  $St > 0.55$ , the wake of the surging turbine is experiencing meandering at a self generated frequency,  $f^*$ , in the range of the natural frequency of the wake of the fixed turbine ( $f^* \in [0.1, 0.5]U_\infty/D$ ). For these cases, the wake's dynamics are more complex, the spectrum shows peaks at  $f_p$  and  $f^*$  as well as mixing components (figure 16 (g, h)). This is an explicit proof of non-linear interactions of these two frequencies, leading to so-called quasi periodicity. In summary, we worked out one dynamic mode for sway (meandering) and two dynamic modes for surge (pulsating and meandering).

These dynamic behaviours play an important role in the recovery process and provide insights into the results observed for the average values. Most interestingly, we see that the synchronisation of the broadband wake modes to the driving frequency leads to a faster recovery. This result seem on a first view counter-intuitive. On the one hand, synchronisation makes the wake structures more organised (i.e. more coherent). In similarity with the shielding effect of tip vortices demonstrated by Lignarolo *et al.* (2015), we could expect less recovery. On the other hand, the pulsating and meandering structures in the wake of the floating wind turbine do not prevent momentum exchange with the flow as do tip vortices, but rather enhance momentum transport and increase the exchange area, thus improving recovery from the wake centre. In a similar way, it is astonishing that the more complex but still low dimensional quasi-periodic states for the surge case lead to an even greater enhancement in recovery (the recovery is about 10 % more for  $St \approx 0.8$  compared to  $St \approx 0.4$ ). Both sideways and fore-aft motions enable the far-wake to be developed closer to the rotor, at  $x \leq 6D$  for the most impactful cases, while it is observed at  $x \approx 10D$  for the fixed case, which is in close relation to the dynamic behaviour of the wake. This study shows that non-linear dynamic phenomena must be taken into account to better understand the behaviour of the wake, especially in the transition region (here  $x \in [3D, 6D]$ ).

The results of the paper demonstrate that perturbations in the near-wake due to platform motions are advected downstream, amplified and interact non-linearly which results in large meandering or pulsating movements in the wake. Interestingly, these motions could enhance the performance of a wind farm by increasing the energy available to downstream turbines. However, it is important to note that the large coherent structures could also contribute to increased loadings on downstream turbines. It is an open question whether or not these features will reduce turbine spacing within future floating wind farms.

**Acknowledgement:** This work has received funding from the EU's Horizon 2020 research and innovation programme under the Marie Skłodowska-Curie grant agreement N°860879 as part of the FLOWAWER consortium. The authors would like to thank Julian Jüchter, Jannis Maus, Dr. Jaroslaw Puczyłowski and Agnieszka Hölling for their valuable help with the experiments.

**Declaration of Interests:** The authors report no conflict of interest.

---

Parameter	Notation	Value	Unit
Rotor diameter	$D$	0.58	$m$
Rotor radius	$R$	0.29	$m$
Hub height	$H_{hub}$	0.96	$m$
Tower length	$T_{length}$	0.45	$m$
Cut-in wind speed	$U_{in}$	2.5	$m.s^{-1}$
Rated wind speed	$U_{rated}$	7.5	$m.s^{-1}$
Rated power	$P_{rated}$	25.4	W
Rotational speed	$\omega$	400-1600	rpm
Tip speed ratio	$TSR$	4-9	[-]

---

TABLE 2. MoWiTO 0.6 characteristics

---

Test	DoF	Amplitude	$A^*$	Frequency	Wind Speed	$St$	$C_T$	$Re$
[-]	[-]	[mm] or [°]	[-]	[Hz]	[m/s]	[-]	[-]	$\times 10^5$
A.1	Fixed	0	0	0	5	0	0.81	2.3
A.2	Sway	4 mm	0.007	3.3	5	0.39	0.81	2.3
A.3	Roll	0.5°	0.007	3.3	5	0.39	0.81	2.3
A.4	Sway	38 mm	0.065	0.3	5	0.03	0.81	2.3
A.5	Roll	5°	0.065	0.3	5	0.03	0.81	2.3
B.1	Fixed	0	0	0	5	0	0.81	2.3
B.2	Surge	4 mm	0.007	3.3	5	0.39	0.81	2.3
B.3	Pitch	0.5°	0.007	3.3	5	0.39	0.81	2.3
B.4	Surge	38 mm	0.065	0.3	5	0.03	0.81	2.3
B.5	Pitch	5°	0.065	0.3	5	0.03	0.81	2.3
C.1	Fixed	0	0	0	5	0	0.81	2.3
C.2	Sway	4 mm	0.007	1-5	5	0.12-0.58	0.81	2.3
D.1	Fixed	0	0	0	3	0	0.76	1.4
D.2	Surge	4 mm	0.007	1-5	3	0.19-0.97	0.76	1.4
D.3	Fixed	0	0	0	5	0	0.81	2.3
D.4	Surge	4 mm	0.007	1-5	5	0.12-0.58	0.81	2.3

---

TABLE 3. Cases investigated. For all cases,  $TSR \approx 6.0$ .For rotational DoFs:  $A^* = T_{length} \times \tan(A)$ .

## Appendix A. Additional data to the experiments



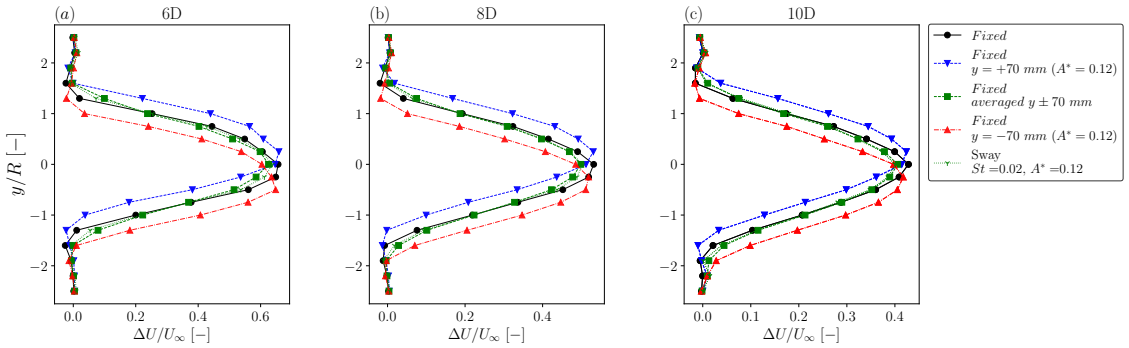


FIGURE 17. Wake deficit profiles at 6D (a), 8D (b), 10D (c) for: fixed case, fixed with an offset of  $\pm 0.12D$  (70 mm) in  $y$  (horizontal), average of the offset cases and sway with  $A^* = 0.12$ ,  $St = 0.02$ ,  $Re = 2.3 \times 10^5$

## REFERENCES

- ACEBRÓN, JUAN A, BONILLA, LUIS L, VICENTE, CONRAD J PÉREZ, RITORT, FÉLIX & SPIGLER, RENATO 2005 The kuramoto model: A simple paradigm for synchronization phenomena. *Reviews of modern physics* **77** (1), 137.
- AINSLIE, JOHN F 1988 Calculating the flowfield in the wake of wind turbines. *Journal of wind engineering and Industrial Aerodynamics* **27** (1-3), 213–224.
- ANGELOU, NIKOLAS, MANN, JAKOB & DUBREUIL-BOISCLAIR, CAMILLE 2023 Revealing inflow and wake conditions of a 6mw floating turbine. *Wind Energy Science Discussions* **2023**, 1–35.
- ARGYRIS, JOHN H, FAUST, GUNTER, HAASE, MARIA & FRIEDRICH, RUDOLF 2015 *An exploration of dynamical systems and chaos: completely revised and enlarged second edition*. Springer.
- BAYATI, ILMAS, BELLOLI, MARCO, BERNINI, LUCA & ZASSO, ALBERTO 2017a A formulation for the unsteady aerodynamics of floating wind turbines, with focus on the global system dynamics. In *International Conference on Offshore Mechanics and Arctic Engineering*, , vol. 57786, p. V010T09A055. American Society of Mechanical Engineers.
- BAYATI, I, BELLOLI, M, BERNINI, L & ZASSO, A 2017b Wind tunnel wake measurements of floating offshore wind turbines. *Energy Procedia* **137**, 214–222.
- BELVASI, NAVID, CONAN, BORIS, SCHLIFFKE, BENYAMIN, PERRET, LAURENT, DESMOND, CIAN, MURPHY, JIMMY & AUBRUN, SANDRINE 2022 Far-wake meandering of a wind turbine model with imposed motions: An experimental s-piv analysis. *Energies* **15** (20), 7757.
- BENZI, ROBERTO, SUTERA, ALFONSO & VULPIANI, ANGELO 1981 The mechanism of stochastic resonance. *Journal of Physics A: mathematical and general* **14** (11), L453.
- BUCKINGHAM, EDGAR 1914 On physically similar systems; illustrations of the use of dimensional equations. *Physical review* **4** (4), 345.
- BUTTERFIELD, SANDY, MUSIAL, WALT, JONKMAN, JASON & SCLAVOUNOS, PAUL 2007 Engineering challenges for floating offshore wind turbines. *Tech. Rep.*. National Renewable Energy Lab.(NREL), Golden, CO (United States).
- CHAMORRO, LEONARDO P & PORTÉ-AGEL, FERNANDO 2009 A wind-tunnel investigation of wind-turbine wakes: boundary-layer turbulence effects. *Boundary-layer meteorology* **132** (1), 129–149.
- CHEN, GUANG, LIANG, XI-FENG & LI, XIAO-BAI 2022 Modelling of wake dynamics and instabilities of a floating horizontal-axis wind turbine under surge motion. *Energy* **239**, 122110.
- DÍAZ, H & SOARES, C GUEDES 2020 Review of the current status, technology and future trends of offshore wind farms. *Ocean Engineering* **209**, 107381.
- ESPANA, GUILLAUME, AUBRUN, SANDRINE, LOYER, STÉPHANE & DEVINANT, PHILIPPE 2011 Spatial study of the wake meandering using modelled wind turbines in a wind tunnel. *Wind Energy* **14** (7), 923–937.

- FARRUGIA, RUSSELL, SANT, TONIO & MICALLEF, DANIEL 2014 Investigating the aerodynamic performance of a model offshore floating wind turbine. *Renewable Energy* **70**, 24–30.
- FARRUGIA, RUSSELL, SANT, TONIO & MICALLEF, DANIEL 2016 A study on the aerodynamics of a floating wind turbine rotor. *Renewable energy* **86**, 770–784.
- FELLI, MAROI, CAMUSSI, ROBERTO & DI FELICE, F 2011 Mechanisms of evolution of the propeller wake in the transition and far fields. *Journal of Fluid Mechanics* **682**, 5–53.
- FONTANELLA, ALESSANDRO, BAYATI, ILMAS, MIKKELSEN, ROBERT, BELLOLI, MARCO & ZASSO, ALBERTO 2021 Unaflo: a holistic wind tunnel experiment about the aerodynamic response of floating wind turbines under imposed surge motion. *Wind Energy Science* **6** (5), 1169–1190.
- FONTANELLA, A, ZASSO, A & BELLOLI, M 2022 Wind tunnel investigation of the wake-flow response for a floating turbine subjected to surge motion. In *Journal of Physics: Conference Series*, , vol. 2265, p. 042023. IOP Publishing.
- FOTI, DANIEL, YANG, XIAOLEI & SOTIROPOULOS, FOTIS 2018 Similarity of wake meandering for different wind turbine designs for different scales. *Journal of Fluid Mechanics* **842**, 5–25.
- FU, SHIFENG, JIN, YAQING, ZHENG, YUAN & CHAMORRO, LEONARDO P 2019 Wake and power fluctuations of a model wind turbine subjected to pitch and roll oscillations. *Applied Energy* **253**, 113605.
- GOUPEE, ANDREW J, KOO, BONJUN J, KIMBALL, RICHARD W, LAMBRAKOS, KOSTAS F & DAGHER, HABIB J 2014 Experimental comparison of three floating wind turbine concepts. *Journal of Offshore Mechanics and Arctic Engineering* **136** (2).
- GUPTA, VIKRANT & WAN, MINPING 2019 Low-order modelling of wake meandering behind turbines. *Journal of Fluid Mechanics* **877**, 534–560.
- HAKEN, HERMANN 2012 *Advanced synergetics: Instability hierarchies of self-organizing systems and devices*, , vol. 20. Springer Science & Business Media.
- HANNON, MATTHEW, TOPHAM, EVA, DIXON, JAMES, MCMILLAN, DAVID & COLLU, MAURIZIO 2019 Offshore wind, ready to float? global and uk trends in the floating offshore wind market .
- HEISEL, MICHAEL, HONG, JIARONG & GUALA, MICHELE 2018 The spectral signature of wind turbine wake meandering: A wind tunnel and field-scale study. *Wind Energy* **21** (9), 715–731.
- HOU, PENG, ZHU, JIANGSHENG, MA, KUICHAO, YANG, GUANGYA, HU, WEIHAO & CHEN, ZHE 2019 A review of offshore wind farm layout optimization and electrical system design methods. *Journal of Modern Power Systems and Clean Energy* **7** (5), 975–986.
- HOWARD, KEVIN B, SINGH, ARVIND, SOTIROPOULOS, FOTIS & GUALA, MICHELE 2015 On the statistics of wind turbine wake meandering: An experimental investigation. *Physics of Fluids* **27** (7), 075103.
- HULSMAN, PAUL, WOSNIK, MARTIN, PETROVIĆ, VLAHO, HÖLLING, MICHAEL & KÜHN, MARTIN 2020 Turbine wake deflection measurement in a wind tunnel with a lidar windscanner. In *Journal of Physics: Conference Series*, , vol. 1452, p. 012007. IOP Publishing.
- HURST, D & VASSILICOS, JC 2007 Scalings and decay of fractal-generated turbulence. *Physics of Fluids* **19** (3), 035103.
- IUNGO, GIACOMO VALERIO, WU, YU-TING & PORTÉ-AGEL, FERNANDO 2013 Field measurements of wind turbine wakes with lidars. *Journal of Atmospheric and Oceanic Technology* **30** (2), 274–287.
- JACOBSEN, ARNHILD & GODVIK, MARTE 2021 Influence of wakes and atmospheric stability on the floater responses of the hywind scotland wind turbines. *Wind Energy* **24** (2), 149–161.
- JONKMAN, JASON M & MATHA, DENIS 2011 Dynamics of offshore floating wind turbines—analysis of three concepts. *Wind Energy* **14** (4), 557–569.
- JÜCHTER, J, PEINKE, J, LUKASSEN, LJ & HÖLLING, M 2022 Reduction and analysis of rotor blade misalignments on a model wind turbine **2265** (2), 022071.
- KLEINE, VITOR G, FRANCESCHINI, LUCAS, CARMO, BRUNO S, HANIFI, ARDESHIR & HENNINGSON, DAN S 2022 The stability of wakes of floating wind turbines. *Physics of Fluids* **34** (7), 074106.
- KOPPERSTAD, KARSTEN M, KUMAR, RAJAN & SHOELE, KOUROSH 2020 Aerodynamic

- characterization of barge and spar type floating offshore wind turbines at different sea states. *Wind Energy* **23** (11), 2087–2112.
- KRÖGER, LARS, FREDERIK, JOERI, VAN WINGERDEN, JAN-WILLEM, PEINKE, JOACHIM & HÖLLING, MICHAEL 2018 Generation of user defined turbulent inflow conditions by an active grid for validation experiments **1037** (5), 052002.
- LARSEN, GUNNER C, MADSEN, HELGE AA, THOMSEN, KENNETH & LARSEN, TORBEN J 2008 Wake meandering: a pragmatic approach. *Wind Energy: An International Journal for Progress and Applications in Wind Power Conversion Technology* **11** (4), 377–395.
- LEE, HAKJIN & LEE, DUCK-JOO 2019 Effects of platform motions on aerodynamic performance and unsteady wake evolution of a floating offshore wind turbine. *Renewable Energy* **143**, 9–23.
- LEIMEISTER, MAREIKE, KOLIOS, ATHANASIOS & COLLU, MAURIZIO 2018 Critical review of floating support structures for offshore wind farm deployment. In *Journal of Physics: Conference Series*, , vol. 1104, p. 012007. IOP Publishing.
- LI, ZHAOBIN, DONG, GUODAN & YANG, XIAOLEI 2022 Onset of wake meandering for a floating offshore wind turbine under side-to-side motion. *Journal of Fluid Mechanics* **934**, A29.
- LIGNAROLO, LEM, RAGNI, D, SCARANO, F, FERREIRA, CJ SIMÃO & VAN BUSSEL, GJW 2015 Tip-vortex instability and turbulent mixing in wind-turbine wakes. *Journal of Fluid Mechanics* **781**, 467–493.
- MAO, XUERUI & SØRENSEN, JN 2018 Far-wake meandering induced by atmospheric eddies in flow past a wind turbine. *Journal of Fluid Mechanics* **846**, 190–209.
- MEDICI, DAVIDE 2005 Experimental studies of wind turbine wakes: power optimisation and meandering. PhD thesis, KTH.
- MEDICI, DAVIDE & ALFREDSSON, PH 2006 Measurements on a wind turbine wake: 3d effects and bluff body vortex shedding. *Wind Energy: An International Journal for Progress and Applications in Wind Power Conversion Technology* **9** (3), 219–236.
- MENG, HAORAN, SU, HAO, QU, TIMING & LEI, LIPING 2022 Wind tunnel study on the wake characteristics of a wind turbine model subjected to surge and sway motions. *Journal of Renewable and Sustainable Energy* **14** (1), 013307.
- MESSMER, THOMAS, BRIGDEN, CHARLES, PEINKE, JOACHIM & HÖLLING, MICHAEL 2022 A six degree-of-freedom set-up for wind tunnel testing of floating wind turbines. In *Journal of Physics: Conference Series*, , vol. 2265, p. 042015. IOP Publishing.
- NEUNABER, INGRID, HÖLLING, MICHAEL & OBLIGADO, MARTIN 2022 Leading effect for wind turbine wake models. *arXiv preprint arXiv:2209.04935* .
- NEUNABER, INGRID, HÖLLING, MICHAEL, STEVENS, RICHARD JAM, SCHEPERS, GERARD & PEINKE, JOACHIM 2020 Distinct turbulent regions in the wake of a wind turbine and their inflow-dependent locations: The creation of a wake map. *Energies* **13** (20), 5392.
- NEUNABER, INGRID, SCHOTTLER, JANNIK, PEINKE, JOACHIM & HÖLLING, MICHAEL 2017 Comparison of the development of a wind turbine wake under different inflow conditions. In *Progress in Turbulence VII*, pp. 177–182. Springer.
- OKULOV, VALERY L, NAUMOV, IGOR V, MIKKELSEN, ROBERT F, KABARDIN, IVAN K & SØRENSEN, JENS N 2014 A regular strouhal number for large-scale instability in the far wake of a rotor. *Journal of Fluid Mechanics* **747**, 369–380.
- PEINKE, JOACHIM, PARISI, JÜRGEN, RÖSSLER, OTTO E & STOOP, RUEDI 2012 *Encounter with chaos: self-organized hierarchical complexity in semiconductor experiments*. Springer Science & Business Media.
- PIMENTA, COIMBRA, MONTEIRO-PACHECO & OTHERS 2021 17th eawe phd seminar on wind energy: Book of proceedings .
- POPE, STEPHEN B 2000 *Turbulent flows*. Cambridge university press.
- PORTÉ-AGEL, FERNANDO, BASTANKHAH, MAJID & SHAMSODDIN, SINA 2020 Wind-turbine and wind-farm flows: a review. *Boundary-Layer Meteorology* **174** (1), 1–59.
- RAMOS-GARCÍA, NÉSTOR, KONTOS, STAVROS, PEGALAJAR-JURADO, ANTONIO, GONZÁLEZ HORCAS, SERGIO & BREDMOSE, HENRIK 2022 Investigation of the floating iea wind 15 mw rwt using vortex methods part i: Flow regimes and wake recovery. *Wind Energy* **25** (3), 468–504.
- ROBERTSON, AMY, JONKMAN, JASON, MASCIOLA, MARCO, SONG, HUIMIN, GOUPEE, ANDREW, COULLING, ALEXANDER & LUAN, C 2014 Definition of the semisubmersible floating

- system for phase ii of oc4. *Tech. Rep.*. National Renewable Energy Lab.(NREL), Golden, CO (United States).
- ROCKEL, STANISLAV, CAMP, ELIZABETH, SCHMIDT, JONAS, PEINKE, JOACHIM, CAL, RAÚL BAYOÁN & HÖLLING, MICHAEL 2014 Experimental study on influence of pitch motion on the wake of a floating wind turbine model. *Energies* **7** (4), 1954–1985.
- ROCKEL, STANISLAV, PEINKE, JOACHIM, HÖLLING, MICHAEL & CAL, RAÚL BAYOÁN 2017 Dynamic wake development of a floating wind turbine in free pitch motion subjected to turbulent inflow generated with an active grid. *Renewable Energy* **112**, 1–16.
- SANT, TONIO, BONNICI, DAVID, FARRUGIA, RUSSELL & MICALLEF, DANIEL 2015 Measurements and modelling of the power performance of a model floating wind turbine under controlled conditions. *Wind Energy* **18** (5), 811–834.
- SCHLIFFKE, BENYAMIN, AUBRUN, SANDRINE & CONAN, BORIS 2020 Wind tunnel study of a “floating” wind turbine’s wake in an atmospheric boundary layer with imposed characteristic surge motion. In *Journal of Physics: Conference Series*, , vol. 1618, p. 062015. IOP Publishing.
- SCHOTTLER, J, HÖLLING, A, PEINKE, J & HÖLLING, M 2016 Design and implementation of a controllable model wind turbine for experimental studies. In *Journal of Physics: Conference Series*, , vol. 753, p. 072030. IOP Publishing.
- SEBASTIAN, THOMAS & LACKNER, MA 2013 Characterization of the unsteady aerodynamics of offshore floating wind turbines. *Wind Energy* **16** (3), 339–352.
- SELIG, MICHAEL S 1995 *Summary of low speed airfoil data*. SOARTECH publications.
- VERMEER, LJ, SØRENSEN, JENS NØRKÆR & CRESPO, ANTONIO 2003 Wind turbine wake aerodynamics. *Progress in aerospace sciences* **39** (6-7), 467–510.
- WIDNALL, SHEILA E 1972 The stability of a helical vortex filament. *Journal of Fluid Mechanics* **54** (4), 641–663.
- WU, YU-TING & PORTÉ-AGEL, FERNANDO 2012 Atmospheric turbulence effects on wind-turbine wakes: An les study. *energies* **5** (12), 5340–5362.